UNIVERSITY OF CALIFORNIA
RIVERSIDE

Rare Earth Cuprate Analysis for High Tc Superconducting Devices

A Dissertation submitted in partial satisfaction
of the requirements for the degree of

Doctor of Philosophy

in

Materials Science and Engineering

by

Stephen McCoy

June 2020

Dissertation Committee:

Dr. Shane Cybart, Chairperson
Dr. Reza Abbaschian
Dr. Boerge Hemmerling

The Dissertation of Stephen McCoy is approved:

Committee Chairperson

University of California, Riverside

Acknowledgments

I would like to thank first and foremost my advisor Professor Shane Cybart. I didn't know where I'd end up but it seems I found a reasonable place. Thank you for letting me pursue personal ideas and giving me the freedom to work how I saw fit. I would also like to thank the post docs I had the pleasure of working under. Ethan, thank you for teaching me all you know about high T_C. I feel like it was just us in the beginning which made my time with you much more appreciative of the knowledge and skill sets you had. Sorry for being a handful sometimes. Hao, you always were up for helpful discussions. If I had an out of sight question you would research it and get back with a response within a day. I always enjoyed running experiments with you, one of the best people to talk to if I needed things explained clearly. You have a unique skill. I would also like to mention Bob Dynes, whom I had helpful discussions from research and jobs to family and home. Thank you for reaching out to perspective lab placements for me. I feel it appropriate to mention my labmates whom I worked closely with everyday for almost 4 years. Jay, Han, Anthony, Yan-Ting, and Yuchao. Because our time together was spent working and collaborating sometimes more than a standard work day I consider you all an integral part of my PhD career. I will miss you guys. Also I would like to thank Ivan Zaluzhnyy from the University of California San Diego, for helpful discussions on XRD and measurements. Finally, I thank my parents Joseph and Cheri McCoy for seeing me through this. Though I thought I was made to work too hard growing up it has taken me until now to understand that was all part of the plan. Thanks Dad, it has paid off. And last, Krystina. Thank you for putting up with a seemingly endless pursuit. From early days as an undergraduate until now. I appreciate it even though I never say it.

To my parents for all the support. Also to my late friend Aaron for making my time out here seem not so far from home.

ABSTRACT OF THE DISSERTATION

Rare Earth Cuprate Analysis for High Tc Superconducting Devices

by

Stephen McCoy

Doctor of Philosophy, Graduate Program in Materials Science and Engineering
University of California, Riverside, June 2020
Dr. Shane Cybart, Chairperson

This dissertation reports on experimental results on growth, fabrication and electrical transport analysis of thin film rare earth cuprate oxide (ReBCO's) superconductors with high transition temperatures. Motivation for these studies exist based on current advancements within the superconducting community with superconducting digital logic circuits, quantum computing, and cryogenic qubit readout and control. These studies of novel films such as HoBCO show high critical current densities of 3MA/cm2 and EuBCO with the highest reported transition temperature of 94K. These film properties rival the best YBCO thin films that are commercially available based upon electrical transport data and surface morphology characterization. Based on these optimal material properties superconducting quantum interference devices were made with improved device performance. It is shown based on the Josephson junction tunneling effect both the critical current values as well as energy gap properties varied based upon different ReBCO thin films. Furthermore, investigations into the effect of substrate matching with the new ReBCO series is shown to exhibit twinning boundary alignment. For film growth a novel method is proven involving an oxygen plasma source used during in-situ oxide sputtering of ReBCOs which as yet has not been reported. With this technique the time required at elevated grow temperatures is decreased which allows for less boundary migration between the substrate and the thin film. Also by controlling the oxygen plasma, elemental oxygen is more easily absorbed into the

lattice during growth which allows quenching of the crystals to room temperature alleviating the need for a high pressure oxygen anneal. Also mentioned are experimental results of creating superconducting vias for multilayer device applications. Superconducting ramps that allow a-b plane electrical transport were developed to better enhance devices such as superconducting quantum interference device magnetometers. Through this experiment previous techniques involving oxygen plasma growth are combined to mitigate ground plane electrical transport degradation brought on by the elevated temperatures required for thin film cuprate growth.

Contents

List of Figures

List of Tables

Chapter 1

Thin Film Superconductors

1.1 Introduction to YBCO

With the discovery of high temperature superconducting oxides such as $YBa_2Cu_3O_7$ (YBCO)[1], oxides have been at the forefront of highT_C superconducting research into applicable technologies and novel devices. However, with the inherent complexity and sensitivity of perovskite structures, development and testing of this material has been a challenging aspect in the field of high $T_C$research. The other major setback was the fact that YBCO needed to be free of defects to possess a high critical current[2]. As with the first high quality films being grown, it had been shown that the critical currents in this material were extremely sensitive to growth procedures. In order to increase the critical current a film with very few defects needed to be created. As a first approach in epitaxial growth, these films were proven to have a critical current enhancement of 2 orders of magnitude above the typical YBCO critical current values at that time[3]. The ability to enhance the critical current range of YBCO with high quality epitaxial films paved the way for the next wave of high T_C research. However, the nature of YBCO itself proves to be the most difficult challenge to overcome.

YBCO is a very complex structure. Starting with the fact that it is a cuprate it exhibits the characteristics of being highly anisotropic[4]. This causes the structure to have

very different electrical transport properties in each direction (the a, b, and c direction in the crystal plane). The b axis within the crystal plane contains copper and oxygen pairs which are thought to harbor electron transport during the superconducting transition of the material[5, 6]. However, with an activation energy on the order of 1 eV, the oxygen atom can be easily influenced to move to an interstitial site within the crystal lattice. Once the oxygen atom is removed from the b-axis consisting of oxygen and copper pairs, the superconducting effects of the material begin to diminish. If enough damage is done to the material, the YBCO loses all superconducting as well as metallic characteristics. Because of the low activation energy of the oxygen, the growth procedures of YBCO and reactions with foreign chemicals inhibit the production processes of clean a-b plane thin film single crystal YBCO substrates. Furthermore, unlike the semiconductor industry, most YBCO growth and processing techniques occur at temperature between 400-750C making them hard to integrate with typical semiconductor processing.

Another problematic step in processing was feature size. Because of the inherent instability of the oxygen copper chains in the lattice, when approaching submicron feature sizes the superconducting properties of the material would begin to degrade. With ion milling, the thermal energy of incoming ionized particles would begin to diminish superconducting properties under 1 micron. As such with wet etching, the limits would approach tens of microns before the chemicals would react with the cuprate and cause a lose of oxygen within the crystal structure.

To circumvent this processing challenge, groups began trying to manipulate the YBCO by causing crystal lattice changes after growth with no chemical etching and low thermal exposure. This next step in research involved an approach in which these high-quality films were bombarded with ion irradiation at varying fluences and different beam sources to test whether a structural change within the perovskite lattice itself would induce a change in the critical current values as well as a shift in the critical temperature. To date this has become the most cost-effective way to manipulate critical currents within High T_c superconducting compounds. In this review we will summarize the overall pathway this

novel idea of ion damaged thin films has taken to get to its current state of development. Furthermore, we will explain the proposed science behind the effect of ion irradiation from GFIS on the thin films themselves as well as new implications into the development of high T_c superconducting devices.

1.2 Detwinned Cuprate Thin Films

Today's current thin films suffer from a major drawback due to the nature of YBCO. The available substrates for growth generally have a lattice mismatch when compared to YBCO. Some of the closest substrate matches such as STO has a lattice constant of 3.905 Angstroms and LAO with a lattice constant of 3.82 Angstroms. YBCO, while matching closely in one direction of the substrate lattice structure will periodically be mismatched in the other direction due to YBCO being a highly anisotropic crystal structure. This inherent flaw in the growth parameters cause the YBCO grown to suffer from a phenomena known as "twinning". This twinning causes grain boundaries to form within the thin film which in turn effects the electrical characteristics of the material. Twinning is an effect that causes two separate crystals to form sharing some of the same lattice points. Rather than a single periodic crystal forming from the substrate, two crystals grow and terminate in different orientations with respect to the original nucleation point. With YBCO, several nucleation points serve to anchor small twinned grains all through out the film. This causes a disordered film to develop across the entirety of the given substrate. When this twinning effect occurs the internal stress of the thin film begin to diminish to some degree. With thin film YBCO growth, these twinning effects cause individual clusters of crystals to form. Given that YBCO is highly anisotropic the electrical properties of the material differ greatly with respect to crystal orientation. A multigrain thin film with varying crystal grain sizes will show exhibit weaker characteristics of superconductivity caused by phase decoherence of the pair wave function. This is due to the fact that when individual grains begin to form with separate crystal orientations, each grain imparts a separate wave function. When the

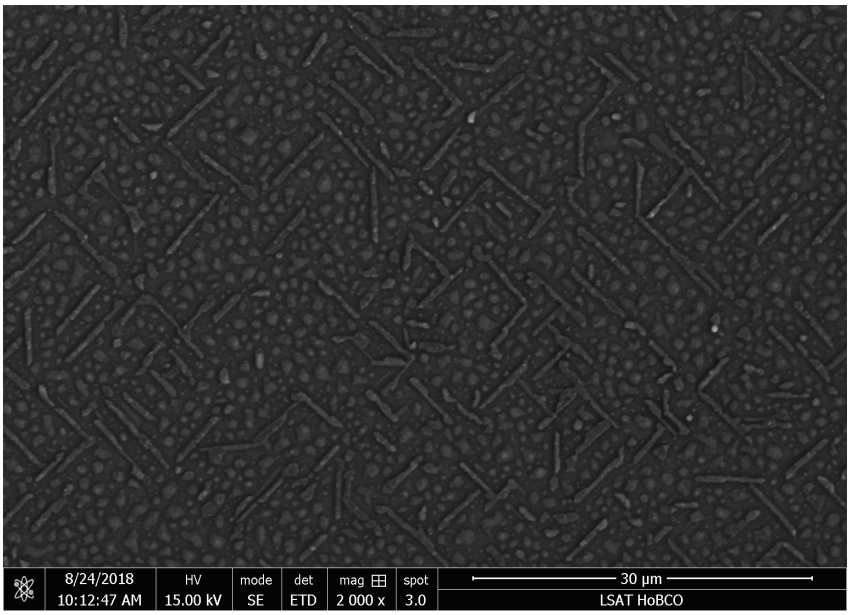

Figure 1.1: Rare earth cuprate thin film grown via off-axis magnetron sputtering. Note the perpendicular formations on the surface. These represent the twinning defects inherent in all YBCO thin film growth. Surface roughness by AFM shows an average of about 20nm.

pair wave function develops across the grains, each grain is slightly out of phase with it's neighboring partner. With multigrain amorphous YBCO the effects are somewhat evened out in a thick film. However if large grains develop separately phase decoherence begins to effect the super conducting properties of the film. With a monocrystalline film, the nature of superconductivity can be more easily studied with respect to known crystal orientation. Novel tests to show d-wave pairing symmetry can then be carried out. Perhaps the most important aspect of the d-wave testing is the fact that it can tell us the symmetry spacing of the crystal orientation. With this known crystal orientation the I_cR_n product of our junctions could be manipulated simply by adjusting the junction orientation within the device. As the feature size of our devices began to shrink there was a noticeable difference in I_cR_n values which was due to varying grain sizes and crystal orientations.

When first investigating YBCO, it was found that the twinning growth nature of the YBCO structure had influence on the transport properties of the material[10]. It has

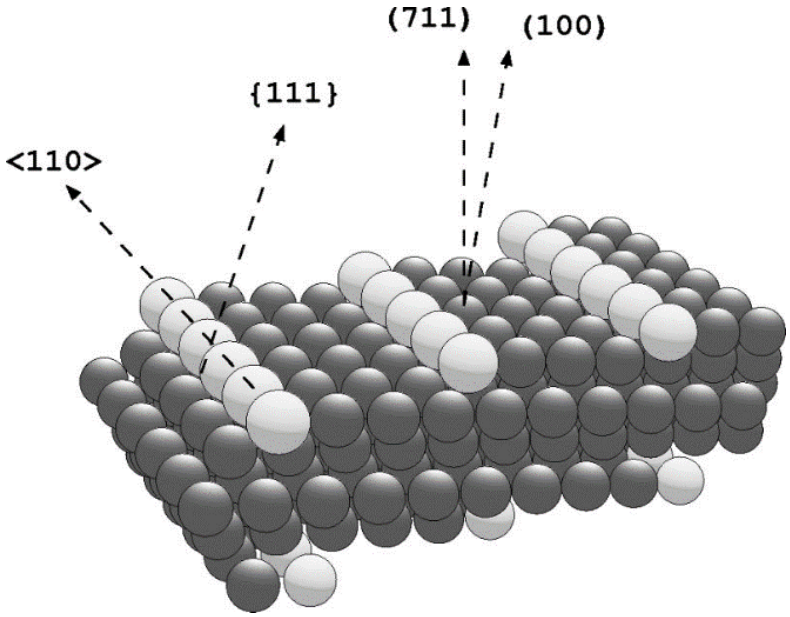

Figure 1.2: An FCC vicinal substrate showing monatomic rows at the (100) and (111) step edge

been described that twined crystal domains serve as flux-line pinning centers[11]. It was suspected that although there is no perfect match for a YBCO substrate lattice, surface modification of the substrates could be one possibility of setting up a preferred stress relaxation point. By doing this, one orientation of the twinning effect would be highly favored over the other. One method of doing this was to break the in-plane symmetry of the substrate (in this case STO) with small miscuts to the substrate in a given twinning direction. By using this technique it was shown that the anisotropic strain between the surface and the substrate was strongly correlated with the detwining of the film[12]. Instead of mirroring the miscut substrates the top growth film had been shifted at varying angles with respect with the normal to the substrate surface. It was shown that when an angle greater than .6deg was used one twin state almost completely dominated allowing for an almost defect free film.

These miscut substrates, usually referred to as "vicinal" substrates require special preparation. A vicinal substrate has a surface that is characterized as having atomic planes

that are stepped at interatomic lengths sometimes resembling a terrace like shape. When a thin film is grown onto a vicinal substrate the interatomic steps serve as nucleation points for growth. When these sites are occupied the orientation of the film lattice is tilted with respect to the normal of the substrate lattice structure. This tilted growth serves as a strain reliever within the film being grown. This tilted structure also allows for an elongated lattice axis which compensates for the substrate and film lattice mismatch. Also important to note, because of this effect the thin film will have a preferred growth direction which mitigates the effect of twinning.

1.3 Ion Radiation Effects

Before the use of GFIS in patterning junctions within YBCO, we will review the brief history of the beginning of ion materials modification. Prior to Ion radiation, junctions made within YBCO were either developed via bicrystal junctions or SNS oxide growth techniques[7, 8]. However, in 1987 Bell Labs filed a patent for modifying a Josephson junction with ion implantation. Further research used ion irradiation on thin film YBCO control the change in critical current brought on by the effects of ion bombardment and varying fluences[3]. Growth of YBCO film was carried out and a set parameter of T_C was measured. These films were then bombarded with Ne ions at 1MeV. A dose of varying fluence was sequentially added in increasing amounts. With each higher dose test a resistance versus temperature plot was made and compared to the previous dose characteristics. Upon reaching a critical dose concentration is was shown that the epitaxial thin film transitioned from superconducting to non-superconducting shown in 1.3.

Furthermore, it was shown that given the magnitude of displacements from the ion concentration dose, it can be calculated that superconductivity can be completely destroyed when the defect density approaches the interatomic length within the crystal at a dose that is of the order 2.2x10^{1}3 $ionscm^2$. This now gives rise to the fact that when YBCO film is exposed to a high enough dose of ion bombardment, the state of the film transitions

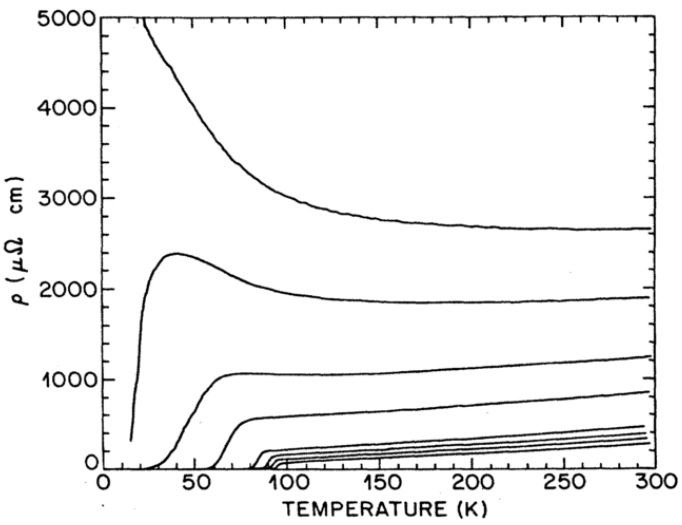

Figure 1.3: A plot representing resistance and temperature at varied fluences. This shows a thin film behavior as it transitions from superconducting to insulating. As the fluence of Ne+ increases the transition temperature decreases and begins to saturate into insulating behavior around 2x10^{13} ions/cm2. Adapted from [9]

from superconducting to non-superconducting[9]. While the transition within the film may seem drastic when considering the electrical properties of the material, the change in the crystal structure itself is much less subtle. Owing to the fact that superconducting pairs were thought to have travelled along the copper-oxygen chains knowing that the superconducting nature of YBCO is very sensitive to the amount of oxygen within the lattice[10, 11]. Another aspect of this study looks at the damage tracks left by ion bombardment of Ne+. By treating these tracks as point defects and calculating a mean separation between the tracks at a given dosage it was found that the critical current dropped just as the separation between the damage tracks approached the coherence length of the superconducting wave function. Furthermore, at higher fluences it was calculated that the damage tracks began to overlap which was believed to allow for flux depinning which causes a lose in superconducting properties[9, 12]. This depinning calculation was shown to correspond to the point where the epitaxial thin film YBCO went from metallic to insulating behavior shown in 1.4.

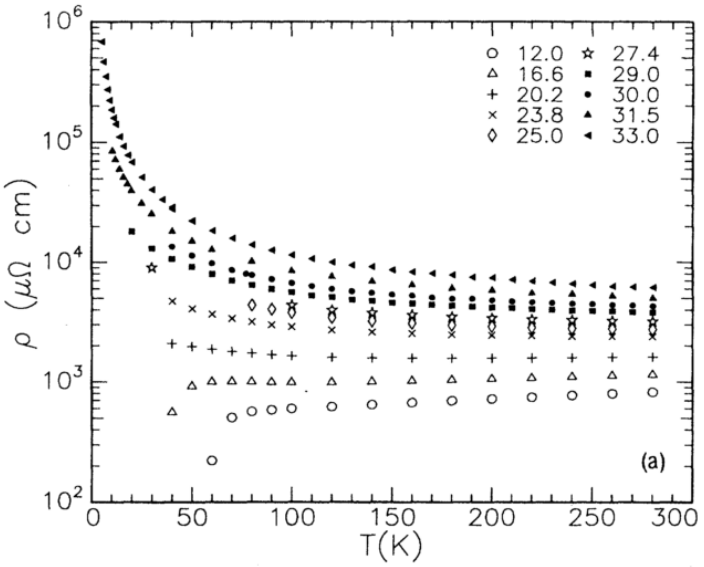

Figure 1.4: This figure shows a plot of high fluence data on a logarithmic scale of resistivity compared to temperature. Shown with varied fluences represented in the top right corner of the graph. Adapted from [13]

By exploiting this phase decoherence a model system was setup to test this theory. In previous work it was shown that phase decoherence was less related to fundamental changes in the crystal lattice. Instead it was thought more to be caused by "islands" with the films grown that shared a loss of coherence throughout the films or by polycrystalline films[13]. If you consider a superconducting wave function

$$\Big\{ \Psi = \delta e^{i\phi} \tag{1.1}$$

Whereas δ is the amplitude and ϕ is the phase, the wave function can be shown to be destroyed either by changing the coherence of ϕ or by suppressing δ. In order to characterize the destruction of superconductivity based on these two parameters the model was developed using a technique known as "quench-condensing"[14]. In this system a conventional superconductor such as lead was thermally evaporated in vacuum and deposited onto a substrate. By cooling the substrate (in this case glass) to cryogenic temperatures

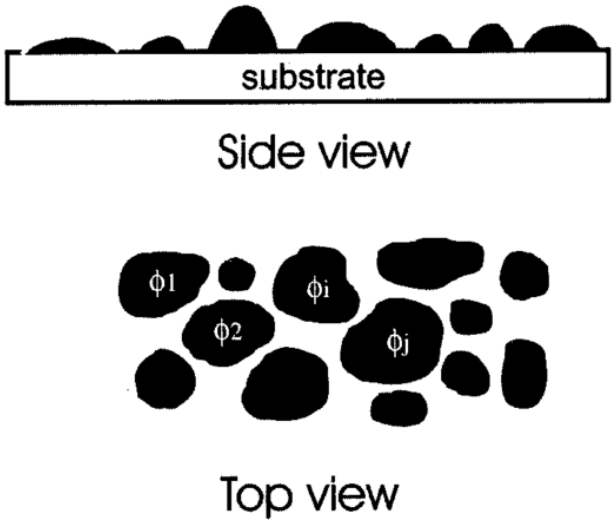

Figure 1.5: An illustration of the grain formation of quench-condensed Pb vapor. By allowing for separate grain formation, each grain possess its own independent superconducting phase. As the grains begin to grow, the proximity effect causes weak coupling. This in turn shows a phase decoherence beginning to develop. Adapted from [13].

(4.2K) the thermal energy absorbed by the lead as it was being evaporated is lost as soon as it makes contact with the substrate. This allows for grains of different crystal orientations to grow and facilities grain boundary formation depicted in 1.5.

When cooled to 7.2K each grain becomes superconducting however, each grain also has it's own individual phase[15]. This can be seen in the superconducting transition of the film in figure 1.4 as being very broad as it approaches 7.2K. Once the transition occurs the individual grains begin to weakly couple and the tail end of the superconducting transition ends at a much lower temperature and begins to broaden out.

In order to study the effects of amplitude suppression of the pair wave function another model system was setup using the quenched condensed thin film growth technique. By "pre-wetting" the substrate with a favorable element such as antimony or germanium the condensation of the lead onto the substrate grew in such a way that the size of the individual

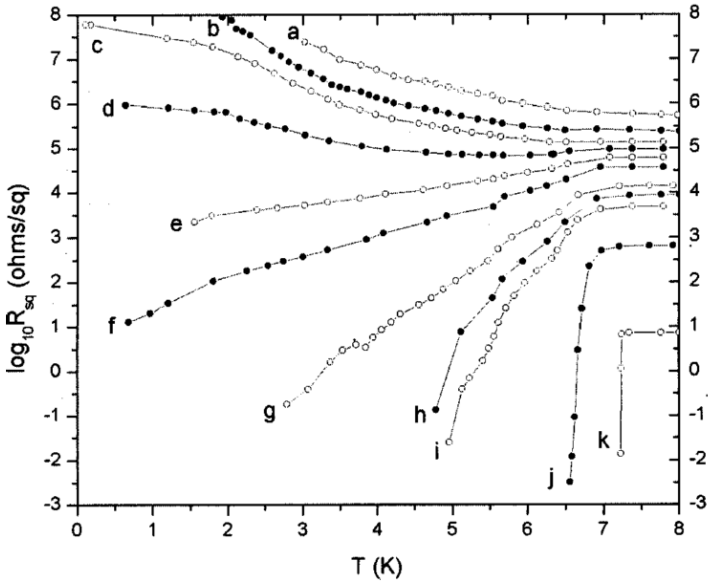

Figure 1.6: This data set represents the resistance and temperature characteristics of the quench condensed Pb film. In sequential order A-K the film is measured in situ as each vapor deposition step is carried out. As shown with the thinnest film (A) the grains are weakly coupled and exhibit insulating behavior. As the grains become larger superconducting fluctuations begin to suppress resistance. Adapted from [13].

grains of lead were much less than the coherence length of the pair wave function. This is due to the fact that the buffer layer allows for lead to form a very thin homogeneous layer similar to amorphous glass[16]. There is no grain boundary formation which completely destroys phase coherence, giving way to an amplitude dominated behavior. As more layers of alternating lead and antimony are added, the superconducting transition remains sharp however the critical temperature rises with each successive layer.

This can be seen as a simple model of a 2-dimensional layer of atoms. The thin layer acts as a grid that limits the mean free path of the electrons to a single plane. As these electrons are confined by a single plane they are forced to interact with each other. Therefore, it can be said that the coulombic interactions negatively effect the amplitude of the pair wave function. This is due to the effect on density of states. As the electrons are confined to a single plane within the film the density of states decreases with respect to film

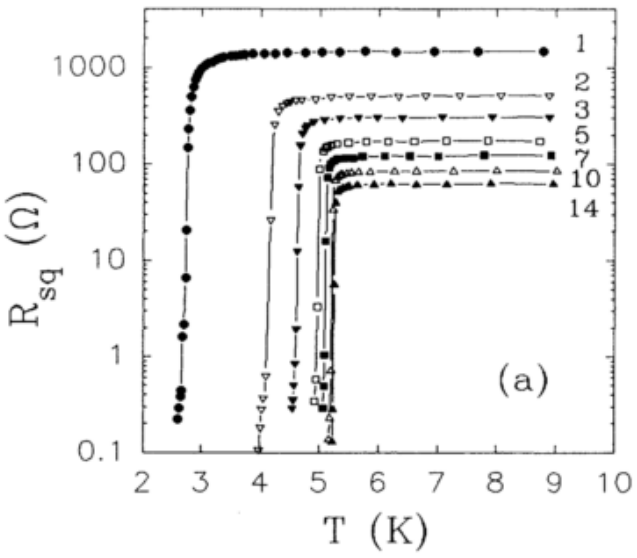

Figure 1.7: A plot representing sheet resistance vs temperature as layers of Pb/Sb are added (1-14). As amorphous layers of Pb are added, the superconducting transition becomes more defined suggesting that amplitude suppression drops out as the coulombic interactions between superconducting pairs becomes less and less of a factor. Adapted from [16].

thickness causing amplitude suppression. This can be seen in equation 1.2

$$\begin{cases} D(E) = \frac{1}{V} \cdot \sum_{i=1}^{N} \sigma(E - E(\vec{\kappa}_i)) \end{cases} \tag{1.2}$$

Where V is the allowable volume, N is the number of discrete states κ is the momentum vector E(κ) is the energy above the ground state. In this equation, while not adapted to 2 dimensional systems, the density of energy states is directly related to the space the pair wave function has within the plane to begin to superconduct.

As the number of weakly coupled layers of lead increase, the coulombic interactions between the electrons becomes less and less which shows in the fact that the amplitude suppression of the pair wavefunction is weakening. Although these tests were done with low T_C superconducting materials, similar effects have been seen with cuprate oxide superconductors with T_C values. As such, this model system can be used to explain effects seen in modified high T_C superconducting materials.

When an oxide superconducting film is exposed to ion irradiation such as Ne+ or He+, characteristics of both phase decoherence and pair wave amplitude suppression is seen. By irradiating YBCO with a known fluence, a plot was made as a function of displacements within the 1st 5nm of the film against the onset of the superconducting transition (Fig 6). As the number of displacements increases the onset temperature transition decreases showing a linear relationship between the two[17]. This pattern shows that pair amplitude suppression is occurring since the transition width remains almost constant. To study phase decoupling of the pair wavefunction YBCO was irradiated and then a plot of increasing fluence against the onset of the superconducting transition temperature for the first 5nm of the film. As shown in figure 7, as the number of defects increases and the transition temperature decreases and there is a broadening of the transition width. This has led to the conclusion that when superconducting oxides are exposed to ion irradiation they exhibit the characteristics of both phase decoherence as well as pair amplitude disruption. From this study, it can be said that the much lighter helium ions exhibit a more uniform impact based on depth of penetration when compared to neon.

Based on the knowledge of previous projects producing near defect free monocrystalline YBCO films is is planned to not only enhance the quality of the films even further but also to utilize known substrates with low dielectric constants in order to apply our films to high frequency applications. The main drawback of all previous methods of monocrystalline film growth known is based on two facts. The first being what is termed as a "film" versus a "thin film". In all other successful published results on monocrystalline films we find that these results are based on films on the order of 100nm or more. It can be argued that the true nature of a defect study on a single crystal would be hard to interpret based on a thicker film. Thicker films tend to have more strain relaxation exhibited through the crystal due to the fact that defects and dislocations tend to happen at the interface of the substrate and film. As the film continues to grow, these interface defects allow for stress relief in each succeeding layer grown. In contrast, with thin films these interface defects are much more prevalent throughout the boundaries of the film (I.E interface to surface)

and cause more strain throughout the entirety of the film. With this in mind, our current processing approach for High Tc junctions is heavily dependent on films that are of a certain thickness (35nm) to allow for successful junction development.

The second problem to be addressed is based on substrate choice and modification. In all other published results on monocrystalline YBCO, the substrates usually mentioned are $SrTiO_3$ (STO) or some variation. This particular class of substrate exhibits a high dielectric constant in nearly all crystallographic directions. While that may not be a problem for certain applications, our model of a High-$T_c c$ device needs to be able to operate at high frequencies. In order to have a reliable high frequency device we plan to first experiment with approaches that have already been mentioned. However, in our study we will first take a look at vicinal sapphire wafers similar to the STO variant. With varying miscut angles with respect to the substrate normal we will RF magnetron sputter cerium oxide as a buffer layer. Throughout the literature it is found that [001] CeO_2 (CeO) growth is needed for epitaxial c-axis oriented YBCO films[13]. This will be achieved by manipulating the temperature of the substrate. Each sample will be tested for correct orientation via XRD. Once the correct grow temperature is achieved growth will begin with YBCO thin films on buffered vicinal substrates via DC sputtering. Through this approach it is hoped to determine weather a vicinal substrate will effect a buffer layer and whether or not that buffer layer will exhibit vicinal properties that will allow for monocrystalline growth. Furthermore, if successful a detemination can be made experimentally about theoretical critical thickness of YBCO on CeO where it is favorable to form misfit dislocations.

Another approach which perhaps offers some of the most promising avenues of success is in using $NdGaO_3$ (NGO) as a growth substrate. With a phesudocubic relationship that matches closely with YBCO (a'=.386nm , b'=0.386nm , c'=0.385nm) NdGaO offers a better lattice match as well as similar thermal characteristics and retains a low dielectric constant. Earlier groups in Germany showed highly ordered films that showed nearly twin-free monocrystalline growth. By manipulating the annealing procedures and nucleation sites

Sample	a-axis (nm)	b-axis (nm)	c-axis (nm)	Therma Exp. $X10^{-6}/^{\circ}C.$
YBCO	3.82	3.88	11.67	16
LAO	3.86	3.82	11.31	10
LSAT	3.86	3.86	3.86	8
STO	3.90	3.90	3.90	10.4
NGO	3.82	3.89	3.85	10
MGO	4.21	4.21	4.21	12.8

Table 1.1: Several ceramic single crystal substrates listed with respect to YBCO. Important to note for NGO, the lattice parameters are based off a 45 ° rotation on the point lattice for YBCO growth. YBCO's high coefficient of thermal expansion is a major obstacle when growing thin films

on the substrate we will try to produce purely monocrystalline films with a film thickness below the critical thickness calculated in earlier experiments.

1.4 Josephson Junctions

Perhaps the most important exploit in designing superconducting electronics is the function of Josephson junctions in superconductors. This junction will be the main focus behind GFIS irradiation. The simple view of this device is two superconducting materials coupled by a thin insulating barrier. In its simple design it lacks the ability to be easily manufactured because of the sensitivity of small changes within the insulating barrier when it is being processed. Before GFIS, manipulating certain process steps in making the junctions[23] would often produce Josephson Junctions however they were not consistent or required lengthy processing procedures. With the fine control of GIFS's sub nanometer beam diameter junctions can be written with a higher degree of accuracy and at a fraction of the cost of traditional Josephson Junction production techniques.

When two superconductors are separated by a thin insulating barrier there exists a phase difference between the coherent wave functions on either side of the barrier. This

phase difference is commonly referred to as the Josephson phase where:

$$\begin{cases} \phi = \delta_1 - \delta_2 \end{cases} \tag{1.3}$$

When a phase difference occurs Cooper pair's begin to tunnel through the barrier when the wave functions begin to develop a current. This is known as the supercurrent. Whereas current flows through the Josephson junction in the absence of an applied potential. This supercurrent can be described as:

$$\begin{cases} I = I_c \sin \phi \end{cases} \tag{1.4}$$

In this equation, known as the 1st Josephson equation[23] the amount of supercurrent that is allowed to flow through the junction is directly governed by the critical current $I_C R_N$ which is often the figure of merit (the product of the critical current and normal resistance) when developing Josephson devices. This critical current value is governed by several factors. Geometry, material quality, and temperature all play a role in determining the critical current value of the junction. When considering the second Josephson equation:

$$\begin{cases} \frac{\partial \phi}{\partial T} = \frac{2e}{\hbar} V \end{cases} \tag{1.5}$$

It can be said that if a potential is developed on each side of the insulating barrier the phase difference of each side is dependent on time. This frequency developed from the phase difference creates an oscillating supercurrent. As seen in the equation above, this frequency is dependent upon the potential developed over the two superconductors. This relation between the voltage and frequency of oscillating supercurrent is known as the Josephson constant. This constant is (483.597879 THz/V) is known as the standard value of a volt. This is taken from the equation above where e is the charge of an electron and $\hbar$ is reduced Planck's constant.

It is important to note that the phase coupling to develop the supercurrent is

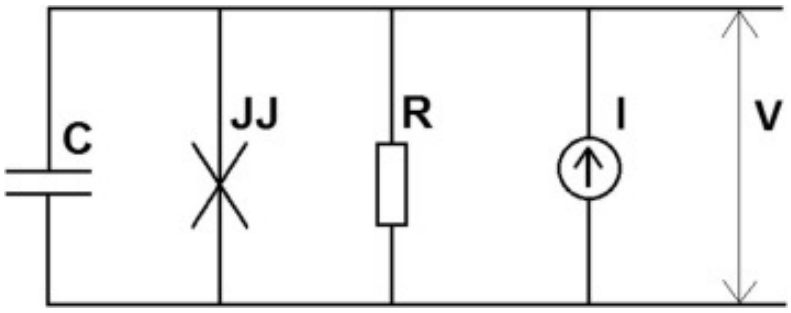

Figure 1.8: The equivalent circuit model of a Josephson junction. Known as the RCSJ model.

directly related to the tunnel barrier width. The inherent short length scale of high-T_C oxides and ceramics is on the order of a few nanometers[24]. This characteristic short length makes the junction extremely sensitive to barrier width. By being better able to manipulate the barrier width, more reliable processing methods can be developed.

1.5 RCSJ Model

In a standard Josephson junction cooper pairs are known to tunnel through the barrier. However, in the standard model quasiparticles (electrons) are also have a probability of tunneling through the junction barrier. In 1968 Johnson, McCumber and Stewart came up with a classical theory to explain and predict this phenomena using classically ohm's law that governed the elements of a resistor and a capacitor in parallel and also a Josephson junction that obeys the two Josephson equations[18, 19]. With a resistor in parallel with the junction (shunt capacitor) and biased the current can be represented as:

$$\left\{ I = I_c \sin\gamma + \frac{\phi_0}{2_N}\frac{d\gamma}{dt} \right. \tag{1.6}$$

With the current split in the equation and a frequency applied to this model the junction has intrinsic capacitance. In this case, a capacitor added is added into the classic model and is commonly known as the restively capacitive shunted junction (RCSJ) model.

The total current that is being passed through the Josephson junction can now be written as

$$\begin{cases} I = I_c \sin\gamma + \frac{\phi_0}{2_N}\frac{d\gamma}{dt} + C\frac{d\Delta V}{dt} \end{cases} \tag{1.7}$$

Now with adding an oscillating current we can substitute the ac Josephson equation (the phase difference in the I_c term) we end up with an equation that resembles the classical kinetic versus potential energy equation.

$$\begin{cases} \frac{\hbar C}{2e}\frac{d^2\gamma}{dt^2} = [I - I_c \sin\gamma] - \frac{\hbar}{2eR_N}\frac{d\gamma}{dt} \end{cases} \tag{1.8}$$

This equation can be seen as a conservative force equation with a dissapative component represented by $\frac{\hbar}{2eR_N}\frac{d\gamma}{dt}$.

This representation resembles a kinetic energy equation with a power dissipation over time. With multiplying the current (I) by the voltage component we can get the power equation over a change in time.

$$\begin{cases} \frac{d}{dt}\frac{1}{2}\left(\frac{\hbar}{2e}\right)^2 C\left(\frac{d\gamma}{dt}\right)^2 + [\frac{-\hbar I}{2e}\gamma - \frac{\hbar I_c}{2e}cos\gamma] = -\left(\frac{\hbar}{2e}\right)^2 \frac{1}{R_N}\left(\frac{d\gamma}{dt}\right)^2 \end{cases} \tag{1.9}$$

Equation 1.9 shows us the kinetic and potential energies established in previous equations relating to the power dissipation on the right and side of the equation which is the power reduction from the series resistor. With the potential energy of the system shown in 1.9 we can now draw a direct relationship between the applied bias current I and the position of our particle in an energy potential and it's behavior when a large bias is applied as opposed to very little bias. This helps to explain the characteristic features of a Josephson junction when a current bias is swept from negative to positive and a voltage readout is recorded.

A typical way to interpret the I–V characteristics of a Junction is to assume a particle in a potential. On this one dimensional potential you have a landscape similar to

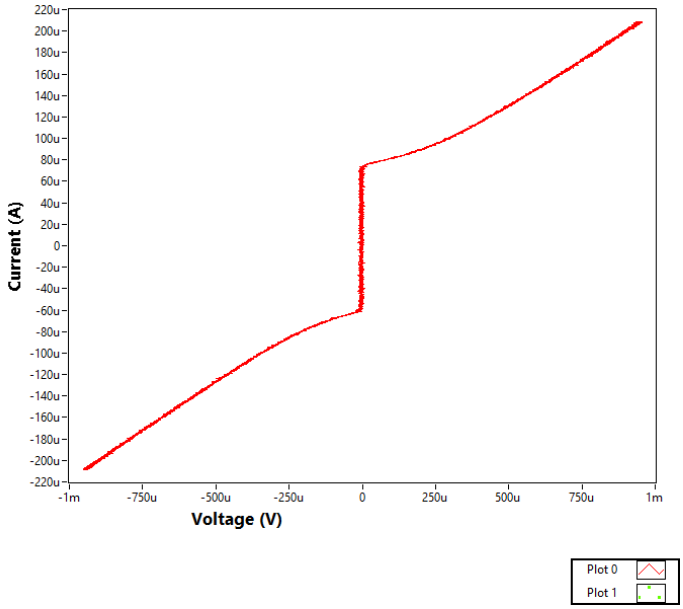

Figure 1.9: I–V plot of a typical Josephson junction. When biased far enough the junction begins to behave linearly behaving Ohm's law but begins to deviate once tunneling begins to occur and critical current is reached.

a washboard. The washboard peaks and troughs serving as potential wells. Depending on where you particle is you may move this washboard potential by tilting the 1 dimensional plane. With respect to to the biased junction, the tilting would come from increasing the current bias through the Josephson junction. When this particle becomes too massive the tilting of the washboard would cause a runaway effect and the particle would cycle across the potential without retaining a fixed position on the potential well. This shows up as a hysteretic loop in I-V plots when the junction becomes too capacitive. In this was, we directly relate the particles fictitious "mass" to the capacitance, C of the junction shown in equation 1.9. Shown in figure 1.9 is an I–V plot of a standard Josephson junction. Here we have a junction with very little excess current showing an over damped junction. Because of this effect, the capacitave term can be negated from the RCSJ model. Josephson junctions that exhibit overdamped properties have the ohmic shunt effect in the charecteristic I–V curves while underdamped junctions exhibit properties of a soft junction that suffer from quasiparticle dissipation at the barrier.

Chapter 2

Oxygen Ion Beam Assisted Deposition of $YBa_2Cu_3O_{7-\delta}$ Thin Films

2.1 Motivation

High temperature superconducting electronics development has been heavily focused on beginning with the discovery of YBCO in 1987 [1]. With the advent of high T_c films over a wide range of materials known as rare earth cuprates came developments in creating Josephson junctions with these new materials. Josephson junctions being the main building blocks of any superconducting circuit require very precise tunnel junctions to be made within the material. Due to the short coherence length of high-T_c materials the junction width is on the order of a few nm[20]. Because of this, thin films used in the creation of high-T_c circuits must be chemically stable as well as very smooth with very few defects. Currently, commercial YBCO films grown on 40 mm sapphire wafers offer a surface roughness of approximately 2 nm but with a temperature independent defect scattering value of around 50 $u\Omega cm$ with a film thickness of 35 nm. These films are generally grown via

reactive coevaporation.

It has been shown that YBCO is inherently sensitive to oxygen content within the lattice structure [21]. One of the challenges of thin film growth of high-Tc cuprates is controlling the amount of oxygen in the crystal during growth to achieve the proper ratio. YBCO is considered an oxygen deficient film when exhibiting optimal properties. The most common method of controlling oxygen content in the crystal is to adjust the partial pressure of the oxygen withing the chamber during growth[22]. Although this is the most used method it has draw backs. As the partial pressure of oxygen is increased during growth, the surface roughness of the film tends to increase[23]. Also a major problem is in the annealing of the sample. At high temperatures and long anneal times cuprate thin films suffer from an increase in surface roughness. Long anneal times are generally done in an oxygen background gas at higher pressures than during growth.

To date there have been several studies that have investigated atomic oxygen exposure to YBCO[24][25]. However none of the studies have been done insitu as we present here. All other studies have simulated grow conditions with elevated temperatures after the sample was allowed to cool and be transferred[26]. For the first time true insitu experimental results are shown.

In this section more controlled ways of introducing oxygen into the lattice during growth procedures are investigated. With the discovery of oxygen ion assisted deposition a system has been developed to take advantage of oxygen plasma from a modified hollow cathode ion gun. By dropping the bias off the extraction grids of the ion gun and flowing oxygen into the body of the gun we can ionize oxygen into monatomic oxygen and flood our grow chamber. Using 4 point vander pauw method measurement there is an increase in T_c as well as decrease temperature independent defect scattering values. Also shown via atomic force scanning electron microscopy (AFSEM) is the improved surface morphology of the films with respect to mean surface roughness. Furthermore x-ray diffraction studies are shown that correspond to the increasing T_c based on oxygen doping.

2.2 Hammond Borrman Model

Based upon previous results, the thermodymanic stability of cuprates has been intensely studied. The growth methods most used include pulsed laser deposition (PLD), molecular beam epitaxy (MBE), metal oxide chemical vapor deposition (MOCVD), and magnetron sputtering. With data from these in situ growth methods a growth chart based on oxygen partial pressures and growth temperatures was plotted. This study was first done by R.H. Hammond and R. Bormann[27, 28]. The Hammond Bormann model is considered the standard while growth thin film cuprates. Within this model there are 4 separate regions separated by thermodynamic stability lines or "phase boundary lines. Each one of these phase boundary lines is represented by experiments conducted with an electrochemical cell that contained Y_2O_3, $BaCO_3$, and CuO. These oxides were baked to 960°C for several hours in oxygen. This provides a stable $YBa_2Cu_3O_7$ compound. When oxygen ions are baked off the electromotive force (EMF) is measured by the Nernst equation

$$\begin{cases} E = \frac{RT}{4Fln\frac{p'_{O2}}{p''_{O2}}} \end{cases} \tag{2.1}$$

where R is the gas constant ($8.314\frac{J}{mol*K}$), T is the temperature of the platinum electrolyte, and F is Faraday's constant ($96.49\text{x}10^3\frac{C}{mol}$). This EMF calculation can be directly related to the number of oxygen ions coming out of the oxygen saturated YBCO and the precised amount of oxygen doping can be determined. This EMF value was measured across a wide temperature range and plotted against the known values of growth parameters. As shown in .

The thermodynamic stability lines represent optimal conditions for the perovskite structure to develop within the cuprate film. On the line, atomic mobility is enhanced giving rise to greater ordering of the lattice structure. As we move further away from the line, the surface mobility begins to decrease. It is important to note that oxygen plays a pivotal role in surface nucleation which leads to a higher number of seed crystals developing

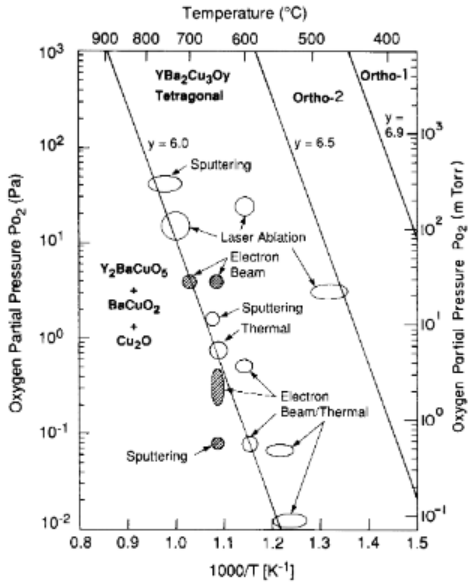

Figure 2.1: This figure represents known grow conditions plotted against thermodynamic stability lines of the perovskite structure in high T_C cuprates. Notice the different phase, from separated oxides to tetraganol and orthorhombic based on oxygen doping. Where y is the oxygen vacancy content. Adapted from[27, 28].

on the substrate per unit time. As expected, this leads to smaller grain size within the film. This model explains the previously mentioned phenomena in the sections. Through this model we will choose optimal grow conditions and compare them when an oxygen plasma is applied to the grow chamber.

2.3 Hollow Cathode Ion Gun Theory and Operation

Standard Ion sources exist on the principal that required an electron source to excite the gas within the gun. Typically the source of ionization comes from cathode filaments that are heated to a temperature that overcomes the workfunction of the valence electrons in the material of the filament. These are known as hot cathode sources. For most materials (typically tungsten is used) this requires energies that cause the filament to become extremely hot and thus, highly reactive. Because of this most ion sources are required to run an inert gas such as argon or nitrogen in order to increase the longevity of the

filament. When the highly energized electrons react with the inter gas, energy is transferred to the gas molecule and an electron is stripped away causing it to have a net positive charge. In order to achieve this interaction, the free electrons from the filament source require a relatively long mean free path. Because of this, most ion sources are required to operate in vacuum. To increase the interaction with the gas and free electrons, the "body" of the gun is housed in magnetic coils or standard steady state magnets. When gas flows into the system it is housed in a main cavity. At the end of the system there are screen plates placed over the body so in order for the gas to escape it must pass through these plates. These plates commonly referred to as "extraction grids" are biased so as to attract or repel positive and negative charges. During excitation of the gas in the system free electrons are generated and need to be removed. Also, atoms that are ionized need to be accelerated out of the system. One extraction grid serves to pull the electrons out of the gas as it passes through. This grid is positively biased and electrons are attracted. The second extraction grid is negatively biased and serves to accelerate the positive ions out through the grid and into the vacuum chamber. These extraction grids serves as a dual purpose element within the system. They can be tuned to not only accelerate the ions but also shape the beam density that exits the system. Depending on which element is being ionized they can also help serve as a capping mechanism to increase ionization efficiency of the gas inside the body. Because of this, it is important to note that modification of the beam can range from having highly charged ions with low current to slightly charged ions with high current. This will be discussed in the coming sections. For ion bombardment purposes such as etching, it is sometimes desirable to neutralize the beam before it reaches it's target. While the beam is generally all ionized still once it leaves the gun a neutralizing element is added inside the chamber to inject electrons back into the beam. Referred to as a plasma beam neutralizer (PBN) this device operates much like the ion source itself.

The PBN consists of a small cavity into which a gas is injected. In the cavity is a hot cathode that gives off electrons when brought up to temperature. As with the ion

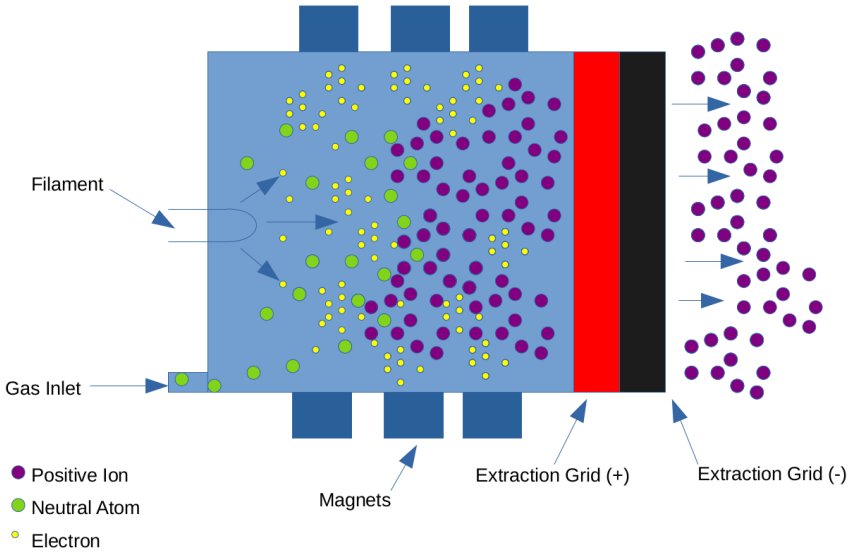

Figure 2.2: A standard modelled thermal ion source. Above pictured is a cross-sectional view of a standard modeled thermal ion source. Current is passed through the filament to release electrons into the body of the source. Inert gas represented by green is flooded into the system under vacuum. The electrons represented by yellow and gas molecules are forced to interact due to the magnetic coils placed around the body. The extractions grids are biased positive and negative shown here in red and black respectively. When the gas molecules become ionized (shown in purple) they are pulled out of the body by the extraction grids and accelerated into the vacuum chamber.

source, the free electrons ionize the gas and the gas is flooded into the chamber. The PBN however does not require extraction grids. When aimed directly into the beam of the ion source the gas floods into the beam and neutralizes and opposing ionized gas it comes into contact with.

2.4 Hollow Cathode Ion Source and Modification

In order to get create a reactive plasma (ionization of a reactive gas such as oxygen) a new source of electrons was used. As mentioned in previous sections, electrons are released from the filament when enough thermal energy is achieved to overcome the work function of that material. Typically for metals these energies are on the order of several electron

volts (eV). Because of this high energy, any filament used to excite a a reactive gas would oxidize quickly and become inoperable. Generally, cathode filaments combine with oxygen and burnout within seconds of reaching operational temperatures.

Hollow-cathode sources operate on a design based around a material with a very low work function. Lanthanum Hexaboride (LAB6) is a typical metal that is utilized for most SEM tips. This material allows for a lower operating temperature when compared to standard cathode filaments such as tungsten. A hollow cylinder of single crystal LAB6 is inserted into a tantalum tube. At the end of the tantalum tube a graphite disc is inserted which allows for the flow of gas with a slight back pressure based upon the porosity of the graphite disk. Surrounding the tantalum tube is an invair heater core wire that wraps around the tantalum tube which is then encased in ceramic to further protect is from oxidation. When current is passed through the invair wire coil it heats up the tantalum tube which in turn heats up the LAB6 core to the thermal excitation state required to overcome the inherent workfunction of LAB6. Free electrons are now present in the tip of the tantalum. An inert gas (in this case argon) flows through the tantalum and meets the graphite tip with slight back-pressure. It is help up within the tantalum tube and ionizes as a result. A small extraction grid or (shell) is positioned on the outside of the graphite tip in order to pull the ionized gas through. This is similar in design to the operation of the previously mentioned accelerator grids discussed in section 2.3.

The main difference in functionality of standard ion sources to hollow cathode source is how they ionize the gas in the body of the gun. When inert gas is ionize in the hollow cathode tip it is extracted out of the tip and into the gun body. To achieve operable pressure with this tip we found that by accurately controlling the distance of the extraction shell from the tip we were able to increase operational pressures by an order of magnitude. Also, in order to further increase differential pressure within the tip itself with respect to the outer vacuum pressure, the graphite orifice was modified to restrict gas flow. This last modification allowed for better ionization of the feed gas without compromising operational pressures.

When the ionized gas enters the body of the gun oxygen is then introduced at a ratio roughly 2:1 oxygen to argon. The highly excited argon reacts with the oxygen to form a mixture of monatomic oxygen (O), ozone (O_3), and oxygen. The gun body material is a quartz bowl that is unaffected by the reactive gases. In using these operating procedures and materials, the heated filament is shielded from the reactive oxygen and can operate for over 1000 hours in optimal conditions. The ionized gas is then extracted and neutralized into the chamber as mentioned in section 2.3.

2.5 Results and Discussion

The first deposition was carried out under optimized growth conditions. This served as the control film for the experiment. After the growth the resistivity vs temperature was plotted. As shown in figure 2.7, the resistivity has been plotted against the other experimental samples.

Sample	Deposition Time (min)	Ion Gun Exposure Time (min)	Surface Roughness (nm)	ρ_o ($\mu\Omega$/cm)	c-axis (Å)
Control	120	0	19.53	102	11.726
Sample 2	120	30	8.80	38	11.714
Sample 3	120	60	7.758	21	11.699

Table 2.1: A representation of the growth parameters relating to each sample and its transport data and surface morphology. The data listed shows a trend in better film quality when compared to length of oxygen ion gun exposure time.

The control sample showed a temperature independent scattering value of $102u\Omega cm$. The transition width was determined by the FWHM of the 1st derivative of the plot. For the control sample a transition width of 1.2K was determined from the plot and T_c was shown at 84K. Upon measuring sample 2 with 30 minutes of ion gun exposure it was found the temperature independent scattering rate had dropped to $38u\Omega cm$. The transition width however increased to 3.6K and Tc remained at 84K. However, with sample 3 exposed for 1 hour to the ion source a transition width of 1.2K was determined with the highest T_c of

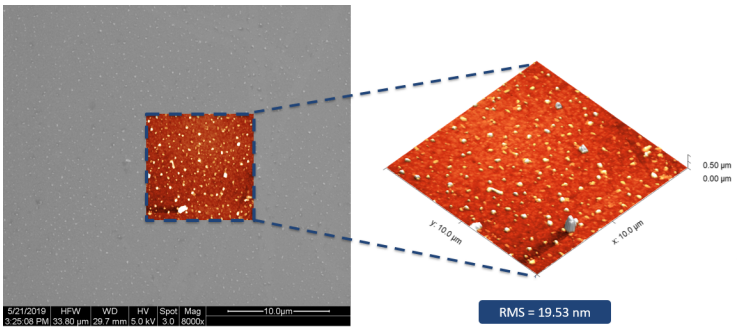

Figure 2.3: The control sample grown with our standard YBCO deposition parameters. This sample exhibits the highest value of surface roughness. However few twinning defects can be seen.

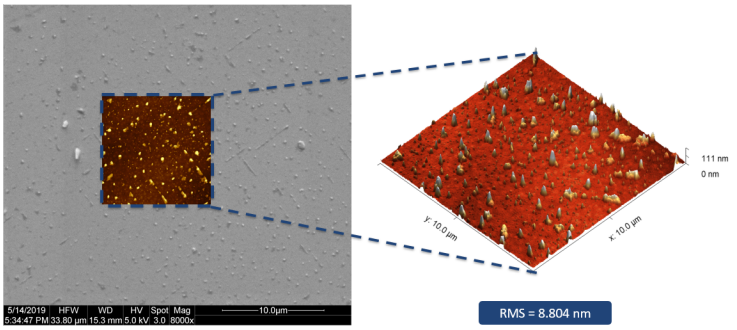

Figure 2.4: 30 minute exposure, this sample shows a reduction in surface roughness. Important to note is the formation of twins shown here as perpendicular striations on the surface.

90K. Most importantly, the scattering rate continued to drop to 21.5 $u\Omega cm$. This transport data clearly shows the film quality increasing with respect to the amount of time exposed to the in-situ ion source.

For surface morphology Quantum Design's AFSEM was employed to obtain a surface roughness value over-layed with high resolution SEM images. As represented in figure 2.7. For the control sample, clear indication of a-axis grain formation can be seen in the perpendicular grain formations on the surface. This indicates stress formations during deposition. This could possibly be due to dislocations within the lattice brought on by lack of oxygen within the crystal. However there have been studies suggesting that thick films

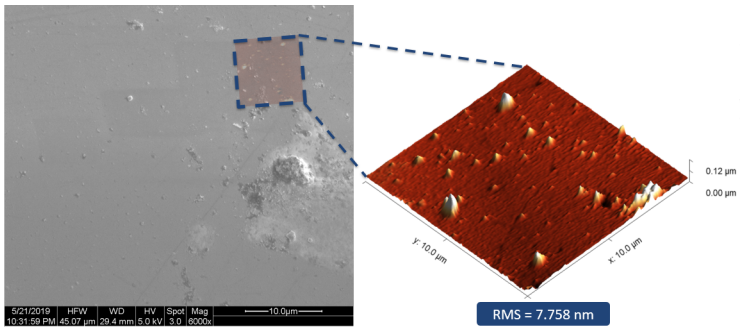

Figure 2.5: The longest exposed of the samples, with a reduced RMS of 7.758-nm there is clear evidence of better surface morphology.

begin to exhibit a-axis growth [29] [30]. The RMS value of the surface was 19.5 nm. Each successive sample afterwards showed clear improved values for RMS in direct correlation with the improved defect scattering rate. The samples exposed to the ion source showed a marked improvement over the control sample with no exposure. Similar results have been shown when samples are annealed in high pressure oxygen. However surface roughness tends to increase with increased oxygen pressure both during deposition and annealing[31]. The 3rd shows the smallest RMS value out of all of the samples. With a mean roughness of 7.7 nm and a line scan roughness of 1.7 nm.

For comparison of the crystallographic features of the thin films x-ray diffraction experiments were carried out on a Rigaku SmartLab system at room temperature using Cu K-α radiation. To determine the values of the c-axis parameter, $\theta - 2\theta$ x-ray scans were measured in the vicinity of (005) Bragg reflection of the YBCO film. Comparing results from the previous measurements, the 30 minute exposure time sample showed the broadest intensity peak where as the control sample showed a slightly narrower peak. This could be due to slight variations of thickness between the films during growth. The 1 hour sample exhibited the sharpest peak among all three samples. This further supports the findings of improved film quality over longer ionized oxygen exposure times. An overall decrease in c-axis parameter was found.

Previous studies show that the c-axis parameter is not only sensitive to defects but

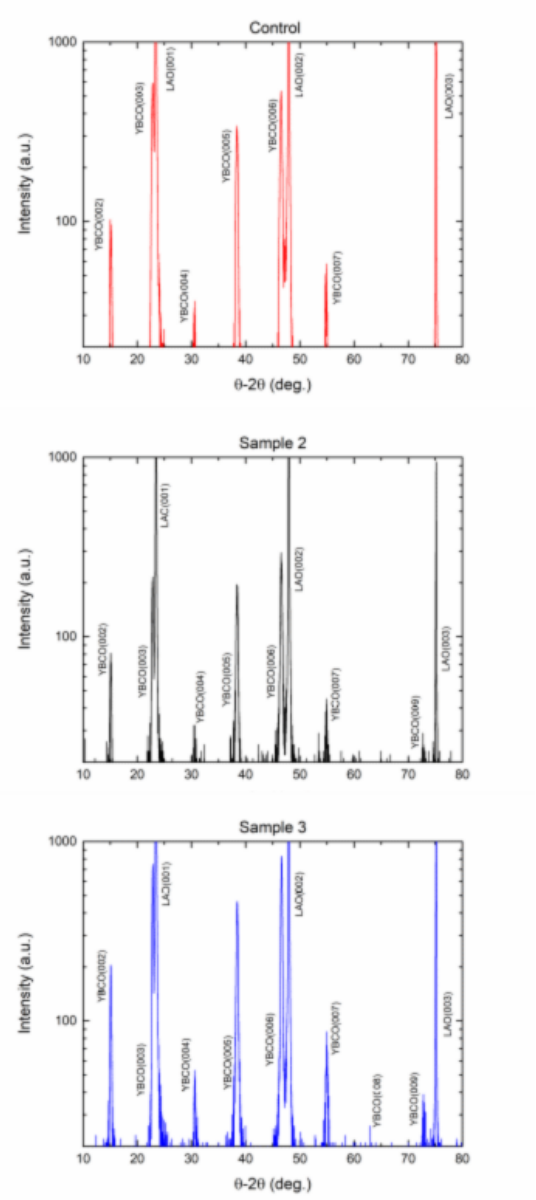

Figure 2.6: $\theta - 2\theta$ scans of the control, sample 2, and sample 3 run respectively. As seen there are sharp peaks of (00l) nature with each successive sample becoming sharper. Also note there are no peaks of (0l0) or (l00) suggesting a single phase crystalline thin film.

also to the oxygen doping content[32, 33, 34]. Aside from our ion exposure it is important to note that the samples also varied with 800 °C exposure times. The samples exhibited superior properties when they were quenched in high pressure oxygen after growth. Other groups have studied this phenomenon and offer the same or similar conclusions[35, 36].

Because of this, we find that the film quality increase is likely due to increased doping via oxygen ion beam plasma. As shown by our diffraction studies, with increasing exposure times to the beam our c-axis parameter decreases from 11.719 to 11.699 Å.

2.6 Conclusion

Thin films samples of YBCO were deposited on LAO substrates via DC sputtering. After a control sample was grown the following samples were grown and exposed to a modified oxygen ion source post deposition for a varied amount of time. Based on the transport measurements and the length of time the samples were exposed to the ion source there was a direct correlation to the decrease in ρ_o. Where as the RMS value also decreases with respect to the control sample. Transition widths were obtained from the transport data and show a slight decrease with an exposed sample whereas the T_C increased as much as 5 K. XRD results also agree with our experimental data. $\theta - 2\theta$ scans were measured for the Bragg reflections around the (005) plane to determine the c-axis length showing an overall decrease in the c-axis lattice parameter further showing the significance of mono atomic oxygen exposure. It can be said that exposure to an oxygen ion source allows for better overall quality films both in surface morphology and transport properties as shown previously in table 2.1. This is thought to be due to the oxygenation of the crystal during post deposition when the ionized oxygen plasma obtains enough energy from the cathode to break down into mono atomic oxygen. Furthermore a novel technique of using a modified ion source has been proven that avoids ion irradiation that would otherwise negatively impact the quality of our YBCO thin films. Future studies are planned for growing procedures utilizing different oxygen plasma sources.

2.7 In-Situ Oxygen Ion Beam Assisted Deposition

A novel method in growing complex oxides in standard growth systems such as MBE is to ignite an oxygen plasma during growth. Recent advancements in ion beam tech-

nology has allowed for higher and higher pressures to be reached all while maintaining a steady plasma. The idea is to not only impregnate the material with monatomic oxygen in hopes that it will have a higher diffusion rate counter to its diatomic cousin when introduced into the crystal. But also that the activated oxygen will fundamentally change the characteristics of the plasma sputter source. Commonly referred to as "Reactive Ion Beam Assisted Deposition" or "RIBAD" groups have been using this method for novel oxide thin film growth[37, 38]. It's predecessor "Ion Beam Assisted Deposition" (IBAD) has also been used for several growth applications[39, 40, 41] as well as target and surface conditioning tools. The main difference being the ion source is run with oxygen as opposed to a non reactive noble gas such as argon or nitrogen.

For our purpose, we have set about growing insitu orthorohmbic YBCO with ignited reactive ion plasma during our sputtering deposition runs. Typical methods as mentioned in the previous section require the film to be deposited. Once the growth has finished the sample is then taken out of the initial growth chamber. It is important to note that in order to do this, the sample must be cooled to room temperature before removal. Also, perhaps as important is the fact the group was required to break vacuum to transfer the samples. Once the samples were transferred they were again pumped down to pressure and heated back to growth conditions further effecting the sample.

To circumvent the previous obstacles that arise during insitu reactive ion beam assisted deposition, we designed a chamber specific to our needs. Low pressure sputter guns were obtained through AJA Int. as well as an ion beam source. This particular ion beam source was designed to excite the gas through RF excitation. Whereby we no longer required a filament. The oxygen plasma source was designed as an RF cavity with magnetic coils to control the shape of the plume. An automatic matching network and 600 watt power supply was used for variable adjustment. Typically the ion source was ran at 13.5 Mhz and 200 watts. This allowed for sufficient ionization of the gas at a flow rate of 10 sccm. In order to test the theory of complete ionization a flow rate was set and the gate valve was positioned and held until a stable pressure readout was reached. The oxygen ion source was

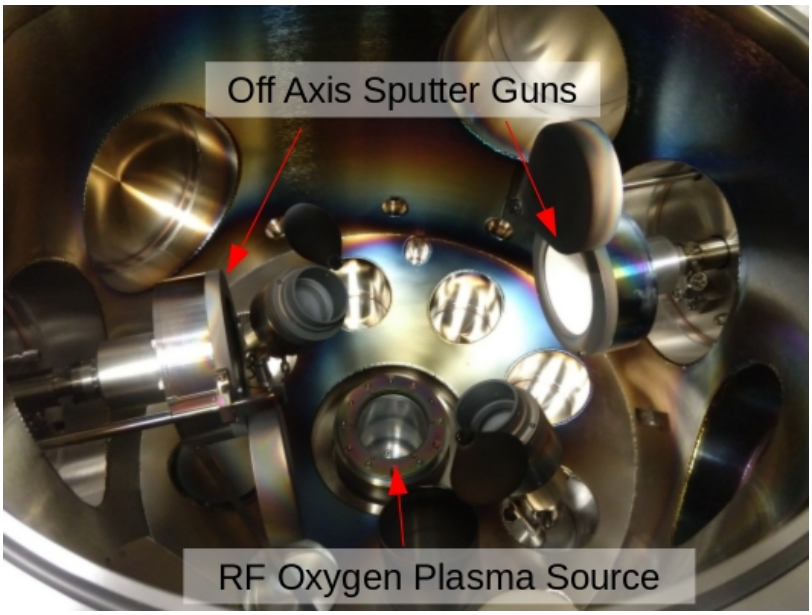

Figure 2.7: A picture of the magnetron sputter deposition chamber. Shown above are the 4 inch off axis guns. Below is the RF plasma generator where oxygen is introduced into the system. Note this is a top down view. The heater and sample holder are lowered between the two guns when the chamber is closed.

then switched on and the pressure reading was again allowed to stabilize. Given the nature of oxygen partial pressure, when oxygen is energized and striped from diatomic to elemental oxygen the partial pressure increases by roughly a factor of 2 based on the ideal gas law and behavior of recombined oxygen plasma [42]. This was seen in our pressure readout when compared to no plasma excitation and was evidence that indeed our incoming oxygen was ionized to some degree.

The chamber setup consisted of two 4 inch off-axis low pressure sputter guns with respect to the center heater. The heater was an incolnel plate with a quartz lamp heater mounted to the back which allowed for substrate rotation. Opposite facing the heater was our 13 MHz oxygen plasma ion source mounted at the bottom of the chamber. This position was chosen with two ideas in mind. A desired effect of the oxygen ion plasma source was to have it interact with the sputter plasma before it reached our substrate for deposition. The other effect being we hoped to partially effect the substrate and film during growth. The

placement of the plasma source enabled us do just that. The pressure was automatically controlled by a VAT feedback servo controlled gate valve backed by a 1000 l/s turbo pump. This gave us precise control in real time to monitor and respond to fluctuations in the base pressure when plasma was ignited or turned off.

Once able to show the ionization of the oxygen source gas, procedures were set to determine the quantitative impact the oxygen plasma source has on our film deposition. A standard film was grown in the chamber with no activated oxygen present. The YBCO target used was prepared by Toshima Materials LTD. and also analyzed by XRD studies to insure our source was of quality. The chamber was brought up to 800 °C with a base pressure of 120mTorr at an oxygen to argon ration of 1:2. The deposition gun was then ramped up to 120 watts and allowed to deposit for 1 hour. The goal was to grow well outside the Hammond-Bormann phase stability lines in order to better understand the effects of the oxygen ion plasma source. This would allow us to compare to diatomic oxygen partial pressures represented on the phase diagram. Once the deposition was finished the chamber was flooded with pure oxygen to a pressure of 300 Torr and the heater was switched off. This served as the control sample.

The second sample was grown in an identical run. However once the substrate was up to temperature and the deposition gun was ramped up, the oxygen ion plasma source was switched on. When the system regained stable base pressure both shutters were dropped simultaneously on both the deposition gun as well as the plasma source. Standard procedures mentioned above were then carried out for the remainder of the grow. At the end of the deposition time both sources were switched off and the standard annealing procedure was followed. When our sample finally cooled we set about to compare transport characteristics of each film. For this a standard vander pauw 4-point method was used.

Resistance versus temperature data was acquired for both sets of samples and compared. It is very interesting to note the change in starting resistance whereas the temperature independent defect scattering rate is almost the same. One possible explanation to

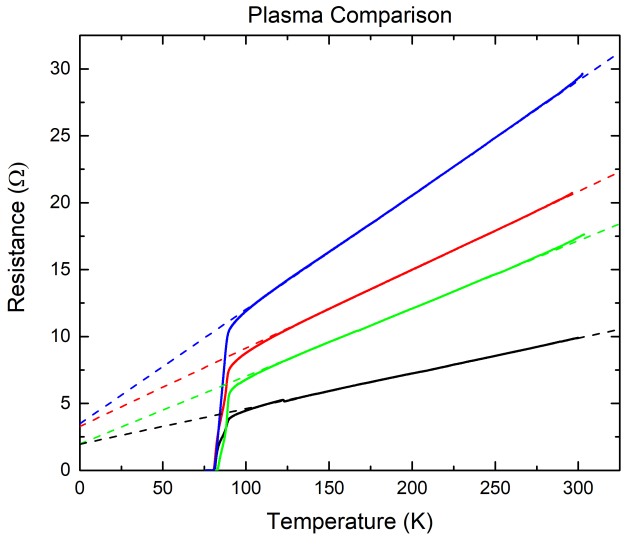

Figure 2.8: Resistance vs Temperature data sets showing plasma growth comparisons as well as plasma distance placements. The Black and red data represents no plasma exposure with black being closest to the sputter gun while the green and blue data set represent growth with plasma, green being placed closest to the sputter source.

this phenomena is that the oxygen plasma impacted the thickness of the film. Upon further analysis via profilometer studies it was shown that the film thickness differed no more than the acceptable margin of error on the measurement system. This showed that the films were near identical thickness. Figure shows transport measurements for the above mentioned deposited films. To mitigate the wide range of substrate positioning on the heater, each run was done with samples placed at the to extremes of the heat. One was placed in the center while the other was placed on the very edge. The black and red data set represent an outside and center sample respectively. These data were of the first sample runs with no oxygen plasma ignited to facilitate pure O_2 growth. Note the increase in extrapolated resistance. The sample placed at the center shows an extrapolated resistance at O K that is 57% greater than that of the sample placed at the edge of the heater. It is interesting to note that, when comparing the exposed plasma samples with the non exposed, the linear fit falls almost exactly on the sample point of the y-axis. This suggests that defect amount

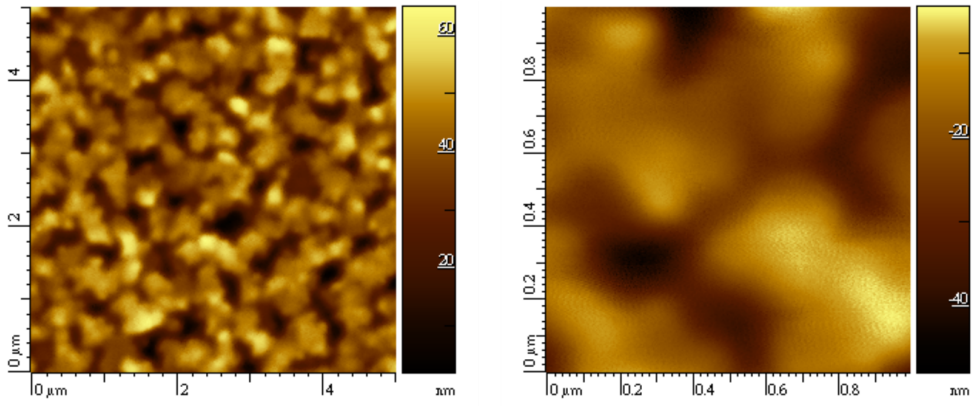

Figure 2.9: AFM scan of inner most sample with respect to the plasma plume. Average surface roughness is 14.8nm. Smoother morphology on the enlarged scan shows no defined crystal structure.

remains the same where as the starting resistance, or composition of the film is more likely effected by the oxygen ion plasma exposure. Upon further analysis we show through AFM scans that the samples placed on the outer edge (close to the deposition gun plume) shown in figures 2.9 and 2.10 show an increase in surface roughness.

These large imperfections in the surface roughness amount to large seed crystals being formed during the early stages of the film deposition process. Because of this, these imperfections serve as defects within the crystal lattice. In previous studies, groups have shown that small defects within the films actually help to facilitate the pair wave function development throughout the crystal and serve as flux pinning centers[43, 44, 45]. These data clearly show a representation of this theory.

Figure 2.11 also shows the samples run with the oxygen plasma source switched on. The green and blue data sets represent these samples in a similar manor as mentioned above. The green represents the out most and the blue represents the sample placed in the center. In comparing with the data sets that have no oxygen plasma introduction we see that starting resistance for the oxygen plasma exposed samples are almost a factor of 3 higher than that of the standard samples. However the extrapolated resistance valves are

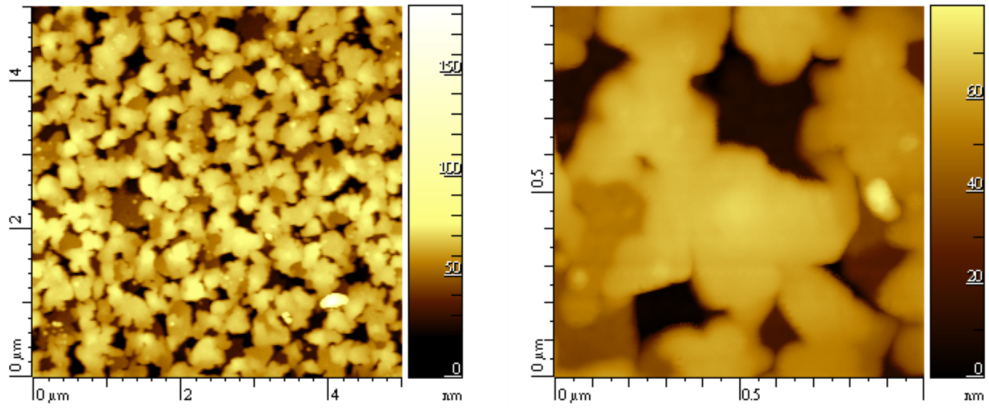

Figure 2.10: AFM scan of the outer most sample with respect to the plasma plume. Average surface roughness is 9.9nm. Almost a 30% decrease from the sample placed closest.

almost identical. This is a very interesting result which indicates that oxygen plasma being introduced into the deposition plume has little to no effect on grain boundary formation. If it were the case, the resistance extrapolation would be adversely effected as grain boundaries serve as scattering mechanisms within the crystal lattice [46, 47]. The other outcome of this experiment shows that T_C of our film increased dramatically over the previous runs. Although each film had a similar onset of around 90 K the transition width decreased by roughly 4 K.

For materials analysis it was important to document the actual composition of our films. To do this each film was loaded into and SEM/EDS system and Energy Dispersive X-ray analysis was carried out. Curiously enough, it was shown through our studies that the oxygen ion beam exposure to growth conditions effected the copper content within the film. Because of the growth setup, it is not known weather the copper was effected in the plasma plume of the deposition gun before it was deposited or if the oxygen plasma somehow effected the as deposited film. We can assume that because the reactive effects of oxygen and formation of copper oxide that the oxygen plasma most likely had a larger interplay with the sputtered plasma rather than with the deposition. Because of the resolution of EDS it was hard to differentiate between substrate constituents and those of which were in the

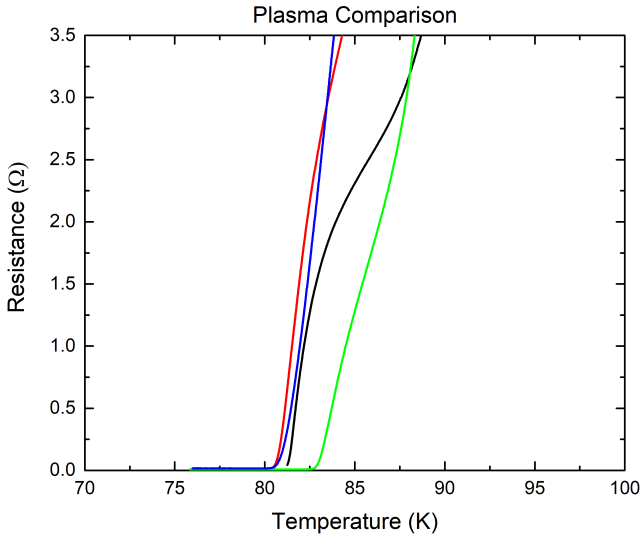

Figure 2.11: Data representing the critical temperature transition widths. Note the decreased transition width of the green data set and also the increase in critical temperature. This is thought to be an outcome of the increase in oxygen doping.

film. The intensity peaks of barium and lanthanum for example could not be differentiated from one another due to a similar atomic mass as well as the gaussian distribution of the x-ray intensity count.

For stoichemetric analysis the SEM/EDS system was setup so as to minimize beam and substrate interaction. To do this, the minimum beam voltage was set to circumvent false reads from our substrate. However, to allow for accurate readout of the ionization information from the thin film beta ionization energies were studied to determine actual stoicheometric ratios. As shown in the following table, general ratios in the EDS mapping suggest an amorphously distributed cuprate. We can see broken down in each layer that none of the main components of the cuprate show uneven density throughout the film. By comparing the ratios between the two films we find that the most effected aside from the copper was barium. As mentioned above, point resolution could not be determined by the SEM/EDS system. However, with correct beam settings and averaging over a large surface we were able to determine two things. The first being that if we were to assume that the

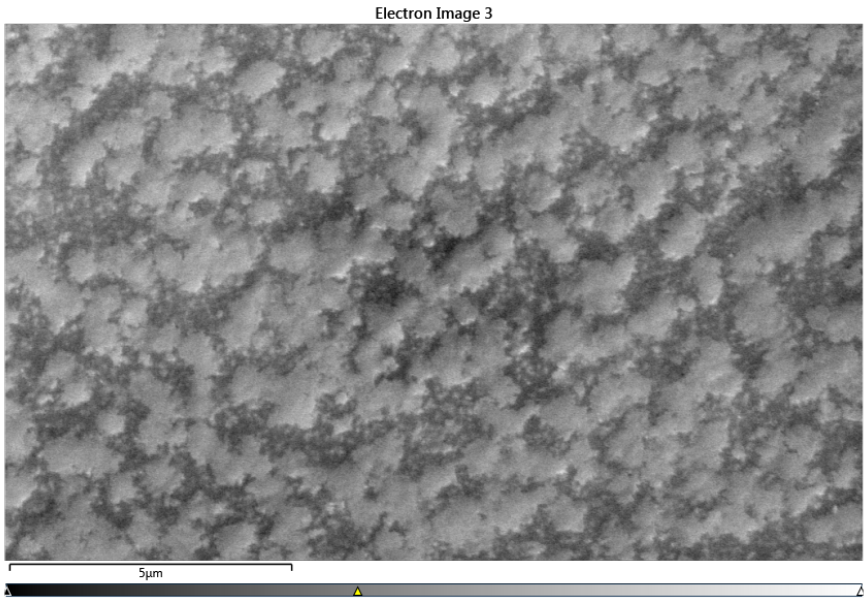

Figure 2.12: An SEM image showing uniform surface morphology. This film was grown with no addition of monatomic oxygen. The plasma source remained off.

substrate content of lanthanum was consistent with each substrate used to grow then a rough ratio of comparison of barium could be deduced from each thin film growth.

This however does not give a correct ratio of stoicheometry within the film but rather a ratio of barium in each grow when compared to one another. Upon this assumption the barium also decreases with the added oxygen ion plasma. It is important to note that the substrates used for this experiment were cut from the same crystal and therefore are in effect identical in all respects. The second is under this assumption we can also get a rough estimate of oxygen content when comparing each film growth.

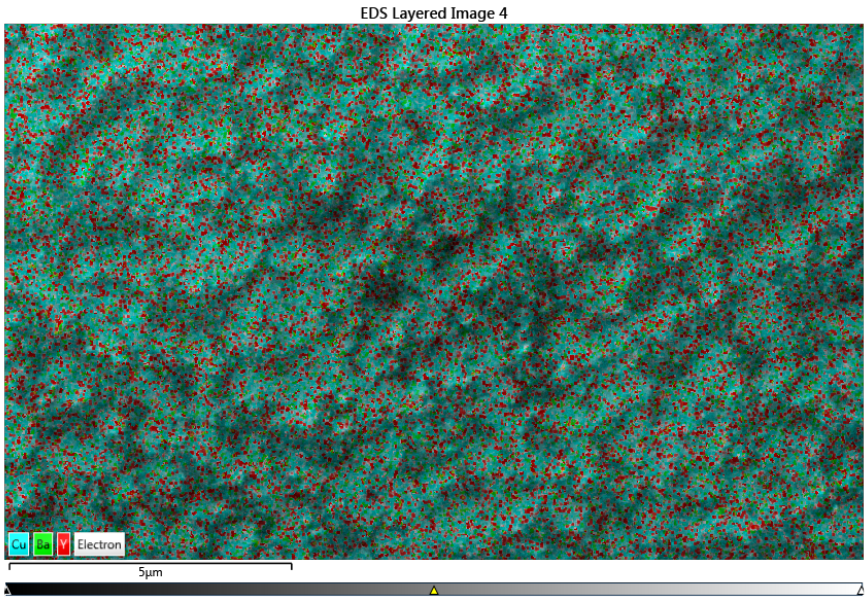

Figure 2.13: A figured depicting the elemental distribution of yttrium, barium, and copper. The film scan shows an even distribution of each constituent with uniform density. This figure coincides with the previous SEM scan.

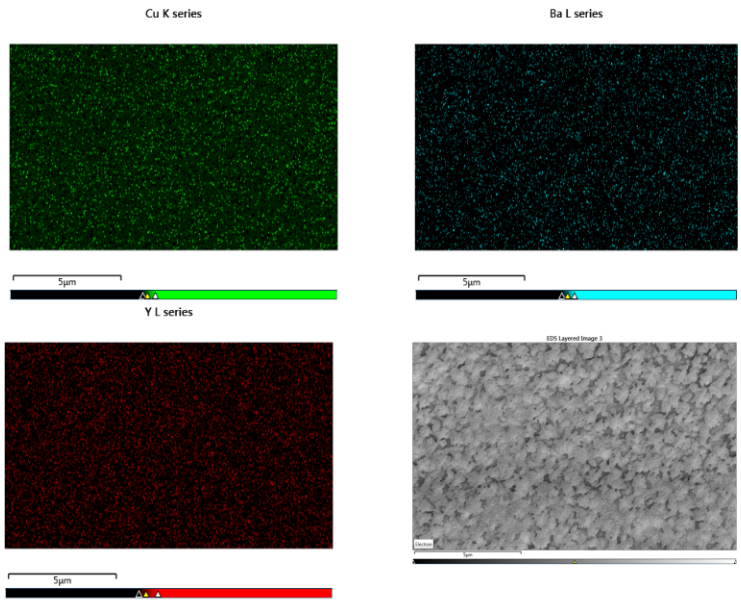

Figure 2.14: An SEM image showing uniform surface morphology. This film was grown with no addition of monatomic oxygen. The plasma source remained off.

Chapter 3

$HoBa_2Cu_3O_{7-\delta}$ Thin Film Junctions

3.1 Introduction

With the discovery of high-T_C materials there has been an ongoing push to create new films as well as improve upon existing film growth procedures.[48] The most commonly studied cuprate YBCO has long been held as the more popular material among scientific researchers since it's discovery in 1987. [1] However, given the nature of cuprates the crystal lattice easily substitutes it's rare earth element (yttrium in the case of YBCO) with a range of rare earth elements. This substitution is thought to effect the Copper oxide chains long thought responsible for facilitating cooper-pair formation and allowing for coherence of the pair wave function through the crystal lattice.[49, 50, 51] As a heavy element such as a rare earth metal is added to the lattice the ionic radius plays a crucial role in the strains built up in the unit cell. By increasing the ionic radius of the element that is binding within the lattice, it is thought that the copper oxide chains undergo an intrinsic strain that forces the chains closer together. This strain and critical current effect has been closely studied in part due to the rise in the use of high temperature superconducting tapes.[52, 53, 54]

Another important feature to note of common YBCO films is the effect of oxy-

gen diffusion at the interface of the substrate and YBCO film itself at high processing temperatures.[55, 56] Studies have pointed out the interplay between highly reactive Barium and other constituents of the often complex substrate composition as a major drawback of growing ultra thing films for devices. The high growth temperatures required for in situ doped film growth allows components to migrate forming unwanted semimetallic compounds which degrade the superconducting characteristics of the film. Similarly, because of interplaying compounds and phases at the interface point defects begin to form which effect chain oxygen order.[57, 58]

To circumvent these problems the replacement of Yttrium with Holmium as the rare earth metal. Holmium possesses unique characteristics when compared to Yttrium. Given that it's ionic radius is much larger than Yttrium.[59] and the binding energies are orders or magnitude higher than that of Yttrium, the aim is to show the effects brought on by the exchanged rare earth metal within the lattice. It is important to note that when comparing YBCO and HBCO as compounds, ionic radius actually decreases. Perhaps allowing for more homogeneous crystalline films.[60]. This suggests that the heavier element Holmium tightly binds the cuprate unit cell closer together when compared to Yttrium. We hope to show through electrical transport measurements the increase critical current values as well as lower defect scattering rates.

A technique described here discusses the epitaxial growth of rare earth cuprate thin films for use with in plane Josephson junctions [61]. Films obtained by DC magnetron sputtering of HBCO have been systematically grown on $SrTiO_3$ (STO), $(LaAlO_3)_{0.3}(Sr_2TaAlO_6)_{0.7}$ (LSAT), and $NdGaO_3$ (NGO) substrates for comparison. It will be reported for the first time the energy gap of HBCO as well as $I - V$ characteristics with response to temperature. Furthermore, it is shown that HBCO is a suitable candidate for high-T_C multilayer devices by employing surface characterization techniques such as SEM and AFM processing to investigate the surface morphology of these films.

3.2 Experimental

LSAT (100), STO (100), and NGO (100) polished single crystal substrates were obtained from Shinkosha LLC. After dicing, the 5 mm x 5 mm samples were mounted to a heater using silver paint as a heat sink. The samples were then baked in 500 mTorr high purity oxygen for 1 hour at 800 C. The substrates were heated from 800 to 825 °C during deposition. A DC magnetron sputtering source was used with a 50 mm HBCO target that had been verified by XRD. The chamber was brought down to 330 mTorr with an Argon to Oxygen ratio of 1 to 1.5 sccm. The Oxygen flow rate was adjusted based upon the characteristics of growth for each substrate to obtain optimal results. Once the chamber settings were stable the DC magnetron sputter gun was ignited and ramped up to 55 watts over the course of 10 minutes. Typical growth rates were around 1 nm/min with a final film thickness of 55 nm. After deposition the chamber was filled with 500 Torr of oxygen and allowed to stand at deposition temperatures for 10 minutes. After, power was cut from the heater and the samples were allowed to cool to room temperature in 500 Torr of oxygen. Once the samples reached room temperature gold was evaporated *in-situ* for contacts.

After deposition the samples were patterned and wire bonded for a 4-point measurement in liquid nitrogen. Once electrical transport was measured and film quality was determined, samples were processed with 2 micron bridges patterned onto the film and milled down to the substrate to make 2 micron bridge test structures. After processing, the samples were written with a Zeiss Orion Plus Helium Ion Microscope with a range of ion doses. The current-voltage characteristics (I-V) were measured for several temperatures to characterize the device properties.

3.3 Results and Discussions

The temperature dependence of resistivity was taken and compared for each growth run. As shown in Fig. 3.3, the transition width of the critical temperature decreases from

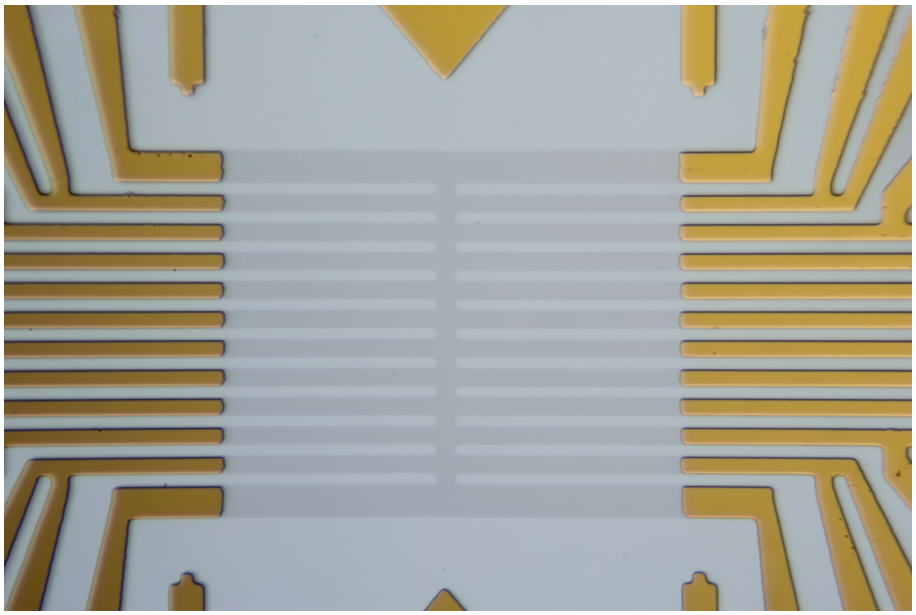

Figure 3.1: A 20 bridge patterened device. Each bridge is shown in the center of the picture. Two columns of 10 bridges. The light blue region with the brides is the actual film with the lightest blue being substrate. The contacts shown on the sides are gold so as to allow for wirebonding. Each bridge is written with varying dosage levels and the subsequently measure for transport and tunneling data.

2.3 to 0.9 K as oxygen is added to the sputter gas mixture. Also we note, when extrapolated to the y intercept a temperature independent defect scattering can be seen. This value also decreases from 35 to 15$\mu\Omega$-cm as shown on the graph. This may be due to fewer defects forming during growth or better ordering of the copper-oxygen chains within the $a-b$ plane of the material. Once grow parameters were determined for each substrate, the thin films were grown and Energy dispersive x-ray spectroscopy (EDS) was taken to insure that the films were stoicheometrically similar to the target analysis. Each film was shown to be within a 5% range of the target data. This falls within the acceptable limit of error for EDS system which is $\pm$5%.

Scanning electron microscopy (SEM) analysis of surface morphologies based upon grow parameters. Based upon higher deposition temperatures spirals begin to form on the surface showing individual grains. With lower temperatures the grains become more scattered with smaller feature sizes. In comparison it can be shown that the films that

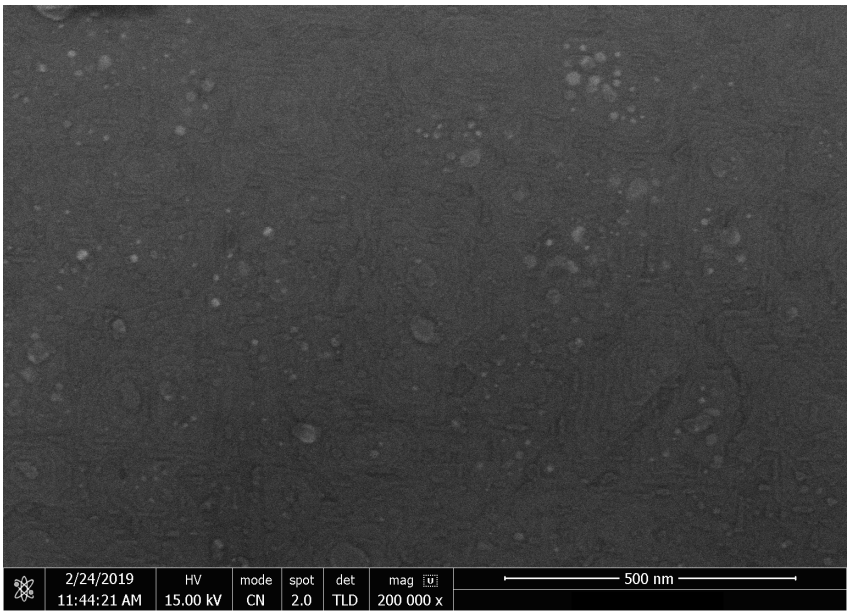

Figure 3.2: An SEM image of HBCO on LSAT. As shown, spirals are able to be seen developing which corresponds to the terrace like growth morphology of HBCO and YBCO. RMS of the film was around 8 nm.

exhibit larger spiral formations within the film matrix have higher critical temperatures.

The best HBCO film produced was grown on LSAT. This film was patterned into 2 micron wide bridges using photolithography and argon ion milling for Josephson junctions. Josephson junctions were written and current versus voltage measurements were taken at several temperatures. Fig. 3 shows (I-V) for one of the junctions over a wide temperature range.

The $I_C R$ is estimated to be approximately 150 $/muV$. The critical current of the junction was measured as a function of magnetic field and is shown in the lower inset. The uniformity of the pattern reveals a uniform current density across the junction. Measurements of the critical current density at 77 K was 3 mA/cm^2 which is in good agreement with prior work [62] and similar to the best films of YBaCuO.

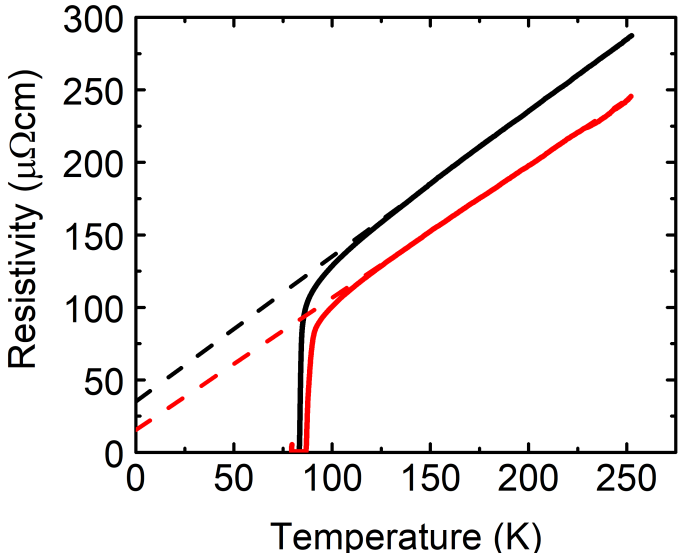

Figure 3.3: A representation of two plots with varying ratios of argon to oxygen during deposition. Note the increased critical temperature between the two plots. The higher oxygen concentrations cause this shift.

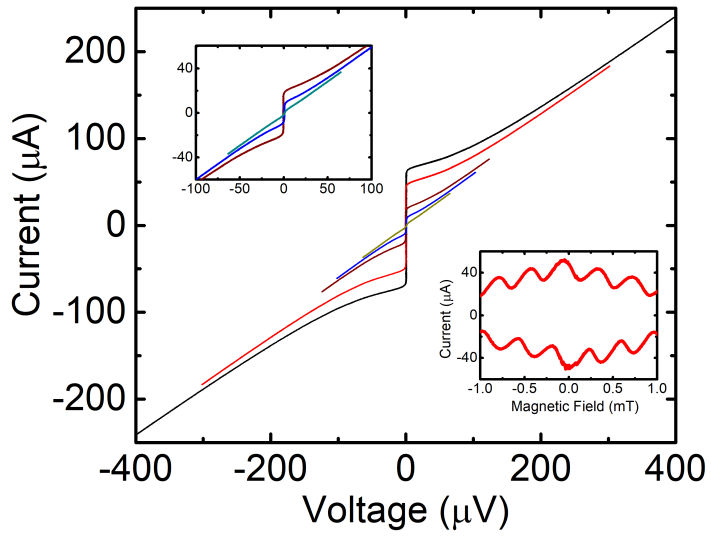

Figure 3.4: A two micron bridge written with a junction thickness of about 2 nm. Current and voltage were measured within a temperature range of 54 to 31 K. At 31 K an electric field was applied to the sample and modulated at 10 Hz. An I_C vs B plot is shown on the lower inset.

Conclusion

The preparation of high-T_C HBCO films has been investigated using off-axis dc magnetron sputtering. Of the different substrates used for growth LSAT (100) has been found to be the best. It can be said that oxygen partial pressure increases critical temperature of films as well as has significant effects on surface roughness of the thin film crystal. It has also been successfully shown fabrication of in plane Josephson Junctions from this material. HBCO shows to be a promising candidate in regards to experimental values compared to YBCO. The critical current densities were a marked improvement over commercially available thin films. The energy gap of this material has been shown for the first time which is in the range of YBCO. Also, ease of controlling surface roughness is an added benefit when looking to apply these films to multilayer devices such as SQUIDS and terahertz antennas. Future work is required to explore this material further to understand more in depth the effects of a larger heavy element replacement for Yttrium.

3.4 $HoBa_2Cu_3O_{7-\delta}$ Superconducting Quantum Interference Device

Superconducting quantum interference devices (SQUIDS) have long been studied for practical applications. Owing to the fact that SQUIDs are the basic building blocks of superconducting electronics, new and ever more sophisticated ways of using SQUIDs and integrating them into complex systems are being established[63, 64, 65, 66, 67, 68]. Because of this, high transition temperature superconductors are once again becoming an intensely studied topic. Dominating the High- T_c field of study are the well known cuprates mainly YBCO. A downfall of YBCO exists in the fact that surface morphology of an epitaxially grown thin film is in direct correlation with transport properties of the material. Generally, as critical current densities increase and critical temperatures increase surface roughness also increases, making for a trade off when considering multilayer devices that require stacked

layers of YBCO The downfall of YBCO is twofold. Owing to the fact that the superconducting copper pairs travel along the copper-oxide chains, a key component in YBCO stability is the binding energy of the oxygen atoms within this chain. The binding energy within the lattice of the oxygen atoms is 0.7eV. This low binding energy causes YBCO to be susceptible to degradation at high temperatures which are required for processing and growth.

To investigate the properties of HBCO such as flux noise and magnetic field response we fabricated superconducting quantum interference devices (SQUIDs) onto our films. We began by patterning devices with pickup loops that varied with respect to surface area. These devices were patterned via laser lithography. Once the chips were patterned and developed we used a bath of KI solution to etch away gold and expose the Ho-Ba-Cu-O film. the remaining gold on the pattern served as contact electrodes for wiring bonding. Once patterned and exposed the devices were loaded into an Argon ion mill and etched for 500 seconds. Because of the large feature sizes within out devices (no less than 10 microns) there was no degradation of film quality due to ion bombardment during etching. The samples were then loaded into our Zeiss Orion Plus Helium microscope. Each Josephson junction was written with varying doses ranging from 600-800 ions/cm2. Figure shows the chip layout. The dashed line represents the tunnel junctions written with Helium microscope. Around the SQUID loop can be seen the flux lock loops.

For device characterization the SQUID was loaded onto a liquid helium dip probe with a u-metal shield and cooled to 4.2 K. The current-voltage characteristics (I–V) were measured for each SQUID with higher consecutive tunnel barrier doses. Shown in figure 3.6 is an I–V at 11K that follows the model suggested by the restively shunted junction model. The junction with the 700 ions/cm2 dose show signs of an insulating Josephson tunnel barrier with very little excess current. The critical current (I_{C}) from figure 3.6 was 150 muA and the voltage state resistance R from the I-V was 2.15 Ω.

For characterization of the magnetic properties of the HBCO SQUID it was biased

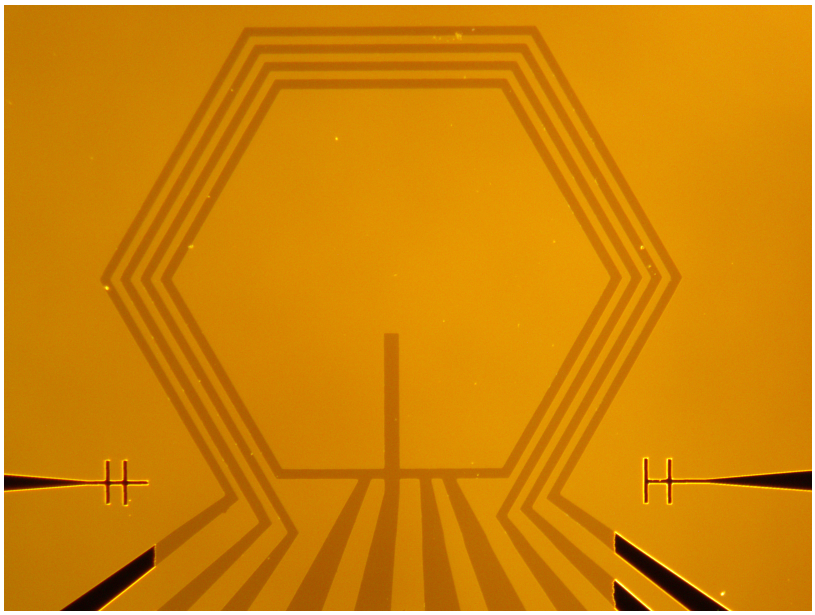

Figure 3.5: The SQUID consisted of a superconducting loop with two junctions written separated by an insulating barrier. The flux lock loops can be seen surrounding the SQUID loop. The lighter lines shown in the photograph is the HoBCO superconducting thin film. The darker regions are gold electrodes that serve as contacts for wirebonding to the chip carrier. The twinned side features serve as symmetry breakers.

out to a set static current of 2.3 amps. The voltage was then measured and plotted while a current was applied to the coil within the probe. The current feed was modulated and the voltage response was observed. Figure 3.7 shows our plotted data from range of 4 μT. As shown, there was a large modulation with an amplitude of 260 μV. The period is shown to be around 1.5 μT. The voltage response data was gathered over a temperature range of 30K. The black data represents 4.2K where as the light blue data set represents the highest temperature of about 40K. Optimal voltage response was shown at about 11K with a response of 260μV. This is in good agreement with values seen with some of the best devices made from commercially available YBCO thin films.

The results from a first ever recorded fabrication and characterization of an HoBCO SQUID show promising results, with slightly higher critical current values than that of the best YBCO films. HoBCO allows us to further extended our applications of SQUIDs for

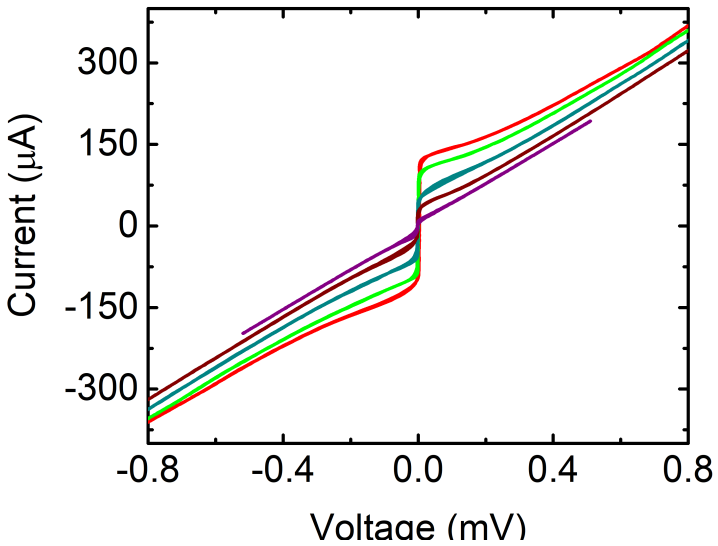

Figure 3.6: A SQUID was measured across a 20K range from 37 to 57K. We show that the SQUID functions over a wide temperature range with a clear indication of superconducting-insulator-superconducting (SNS) junction characteristics. Because of the background magnetic field we modulate the b-field within the probe to average out against background magnetic field. The junction was written with a moderate dose of 600 ions/cm^2 .

a wide range of devices such as multilayer flux couple SQUIDS, magnetometers as well as amplifiers to bridge the gap between superconducting electronics and the read out circuits based off of high impedience silicon devices. Our noise measurements show a marked improvement over what has been previously published. And while the magnetic field response shows no improvement over other SQUIDs developed on similar material it can be said that there is also no lose in performance. From a device fabrication and development standpoint, HoBCO will open up new avenues for multilayer processes given its ease of deposition with a resulting smooth film when compared to YBCO. Future works are planned for ramp vias for multilayer applications.

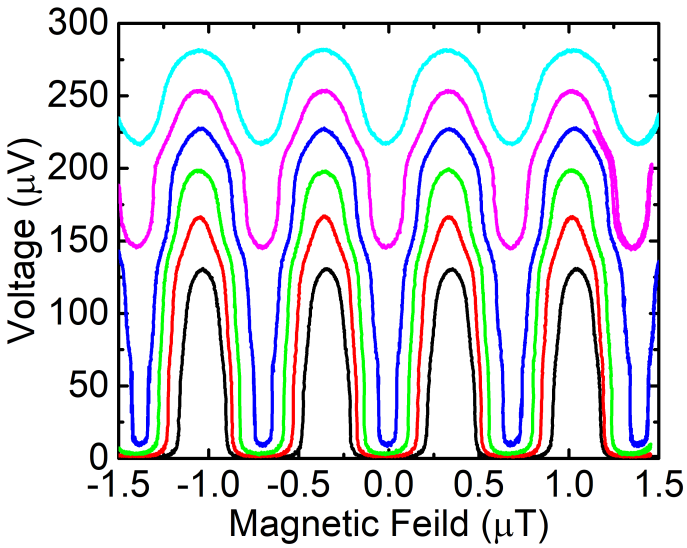

Figure 3.7: A voltage vs magnetic field response is shown. An on chip coil was used as a flux focusing ring as a current was applied and modulated with respect to time. At 11K the SQUID shows a voltage response of 260 μV with a period of 1.5μT.

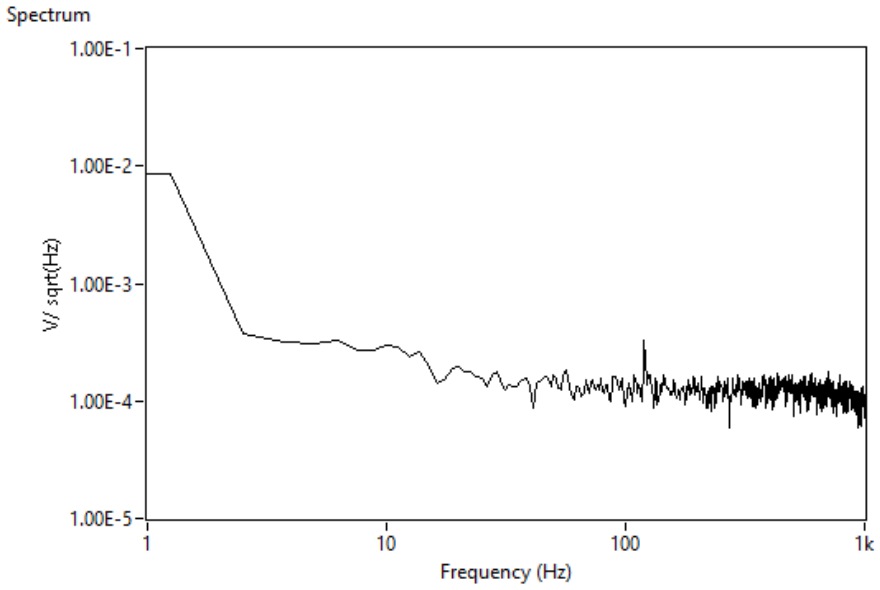

Figure 3.8: A noise measurement made of the HoBCO SQUID. The SQUID and showed good modulation. Once locked the frequency was swept from 1 to 1kHz. This low noise device outperforms an device fabricated in YBCO to date.

Chapter 4

Rare Earth Cuprate Growth and Analysis

4.1 $GdBa_2Cu_3O_{7-\delta}$ Growth and Characterization

$GdBa_2Cu_3O_{7-\delta}$ (GdBCO) is one cuprate studied that has one of the smallest ionic radii for it's rare earth element (gadolinium). This is expected to suppress the critical temperature of GdBCO and therefore lead to lower critical current densities. Recently, with the advent of superconducting strips for power transmission GdBCO has came into focus as a potential candidate for superconducting strip coatings. Because of the high nucleation rate during deposition, GdBCO coating would prove to be an easily produced coating on an industrial scale. In previous reports, it had been found that contrary to the theory of suppressed critical current densities, GdBCO actually exhibits higher values for critical current densities when compared to YBCO[69]. This is thought to be an effect caused by the substitution of Gd onto the Ba sites within the crystal lattice. More importantly, GdBCO has been shown to exhibit controllable a-axis or c-axis growth during deposition based upon the saturation rate of Gd and Ba substitution. This phenomenon may be useful in studying b-axis in-plane transport and tunneling properties. Due to the constraints of the substrate lattice parameters, aligned epitaxial a-axis film growth would occur whereas

with c-axis, because of the closely matched dimensions of the b and a-axis with the cuprate, misorientation onto the substrate often occurs resulting in an amorphously twinned film.

For growth procedures a GdBCO target was obtained from Toshima Manufacturing Ltd. with a stoicheometric ration of 1:2:3 with respect to gadolinium, barium, and copper. The phase orientation of the target was verified by XRD analysis. As with previous film deposition parameters we started with the optimal known growth conditions for YBCO. Our RF megnetron sputter gun was used instead of our DC source. This ensured no target arcing during initial growth trials. A ration of 2:1 argon to oxygen was used as with YBCO. The only difference in growth parameters normally used was the deposition time. By running for 90 minutes we tried to compensate for the slow nucleation rate. However, during our first attempts we noticed very little deposition when we unloaded the chamber. Keeping everything constant we slowly increased our deposition time until we were able to achieve our standard thickness of our in house films which was 55nm. Although these films exhibited fair qualities when considering critical temperature and room temperature resistivities they unfortunately had to be held at elevated growth temperatures for a prolonged period of time. It was observed that the first successful films required deposition times of almost twice that of our other cuprate growth parameters as well as a substrate temperature of around 820°C.

To reduce the exposure time of the sample it was decided to elevate the substrate heater temperature even more. This allowed for a decrease in deposition times down to 1 hour. All while maintaining our desired 55 nm film thickness. The final growth parameters were as follows. The RF power on our sputter gun was set to 120W with an argon to oxygen ration of 2:1.5. The base pressure was 30mTorr while the substrate heater temperature was around 835°C. The deposition time was 1 hour. Once the gun was ramped down the chamber was back-filled with pure oxygen to 300 Torr. Once the pressure stabilized the power was cut from the substrate heater and allowed to cool to room temperature before being removed. It is important to note that because of our water cooled quartz lamp heater,

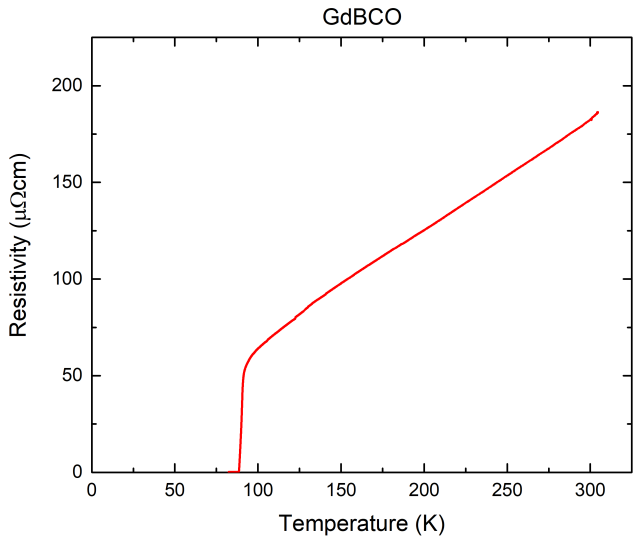

Figure 4.1: Transport measurements showing GdBCO on LAO. Residual resistivity is $3.27\mu\Omega$cm with a critical temperatures around 89 K.

the sample was rapidly cooled to room temperature usually within 25-30 minutes.

After characterization of the films via 4 point method in liquid nitrogen the samples were then patterend with our standard 20 bridge sample style via photolithography. Because the films were slightly thicker than our standard commercially available films we wrote out junctions with slightly higher fluences. The typical dose range that has viable tunnel junctions is usually 300-800 ions/cm^2. For our GdBCO sample anything below 450 was too light of a dose and anything above 650 created an insulator.

Figure 4.2 shows a junction written at 550 ions/cm^2. The temperature range that critical current in our tunnel junction began to appear shows very similar results to a tunnel junction written in YBCO. However, the YBCO junction requires a lesser fluence. We also saw that our normal state resistance was significantly higher than that of YBCO junctions. This could be attributed to the junction properties itself. Further analysis with junctions at even higher fluences are needed to investigate this phenomena further to determine if it is indeed junction related or an artifact of material property.

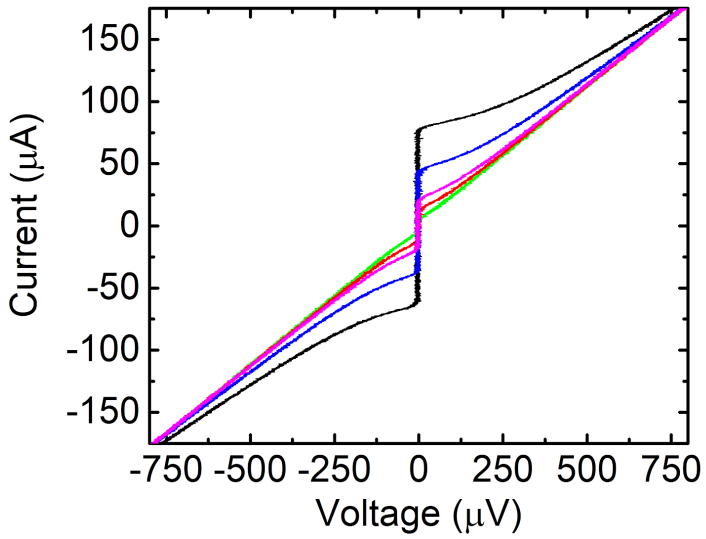

Figure 4.2: I–V characteristics of a biased Josephson junction written in GdBCO. The black data represents a sweep at 4K while the green data shows a sweep at 50K.

4.2 $NdBa_2Cu_3O_{7-\delta}$ Growth and Characterization

$NdBa_2Cu_3O_{7-\delta}$ (NdBCO) in the series of ReBCO's differs from the other aforementioned cuprates in several respects. Most importantly, samples of NdBCO show surprisingly high transition temperatures of around 94 K for thin films and bulk samples reaching as high as 98.7K[70, 71]. Also, it has been shown to have a significantly higher critical current density than that of YBCO[72]. Of the rare earth cuprates, NdBCO exhibits higher surface stability than standrad YBCO films as well as better crystallinity and almost atomically smooth surface morphology[73, 74]. Because of this, NdBCO would seem a promising candidate for our energy gap anisotropy studies. However there are some drawbacks. Part of what makes NdBCO unique is in the fact that neodymium and barium interplay during growth and do not form a solid thermal stability line compound[70]. Instead, the formation of $Nd_{1+x}Ba_{2-x}Cu_3O_{7-\delta}$ where as "x" is a substitution of either Nd or Ba site atoms. This is because when barrium forms an ion Ba^{2+} and neodymiun forms its ionic equivalent Nd^{3+}, they become easily interchangeable within the crystal lattice. This amount generally

varies less than 0.1. However, it has been shown that even minute substitution between these two atoms drastically effects the high transition temperature of this compound. Given neodymium and barium share a very similar ionic radius this could be there reasoning behind the interplay between these two atoms within the crystal lattice during deposition. Because of the larger ionic radius of neodymium compared to YBCO, it is as expect that critical temperature should go up. It has been proposed that the reason there is very little surface degradation is because of the active component of the system barrium is not as readily available on the surface of the material. Studies have shown that the barium oxide plane of the lattice in cuprates reacts with air[75, 76]. This causes a drop in film quality. Because of the interchangeable ions Ba^{2+} and Nd^{3+} less barium is thought to be available at the surface when compared with YBCO and other cuprates.

As proposed in early literature, the effect of a larger ionic radius in the 123 cuprate compounds is thought to have a similar effect to that of stressing superconductors to acheive higher critical temperatures. Just as bulk samples are compressed or strained, when an element is introduced into the cuprate with a larger ionic radius, it stresses the lattice and aids in copper-oxide chain compression. This is thought to be the mechanism in which critical temperatures rise for cuprate thin films and bulk samples[77]. Also important to note, because of this solid solution compound of $Nd_{1+x}Ba_{2-x}Cu_3O_{7-\delta}$ depositing this film is extremely sensitive to slight changes in growth conditions. As other groups have found, we show that sufficiently lower oxygen pressures are required to grow high quality NdBCO films[72, 78, 79]. Based upon the standard Hammond and Bormann line $1/T - log[P(O_2)]$ our growth stability line shifts to the left. This allows us for better control of oxygen growth as well as shortens the time required for holding our samples at deposition temperatures, further mitigating interface boundary diffusion between the substrate and film.

It has been proposed that the reason the surface does not degrade is because of the active component of the system barrium is not as readily available on the surface of the material. Studies have shown that the barrium oxide plane of the lattice in cuprates reacts

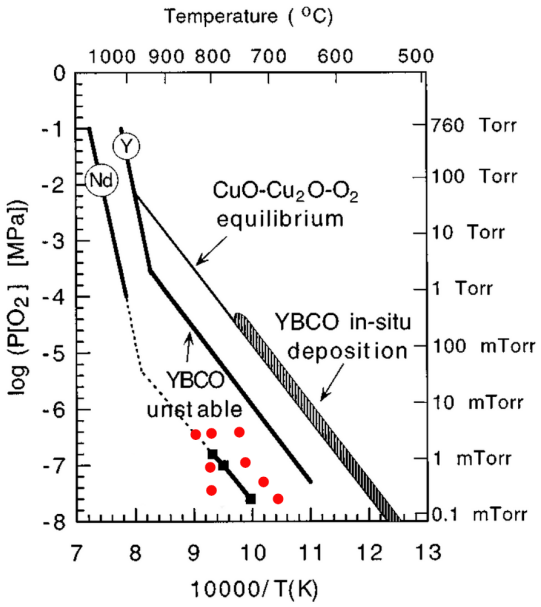

Figure 4.3: Shown above, a modified version of the Hammon-Borman model. neodymium solid phase line runs slightly shifter to the left due to a higher melting point. Growth parameters attempted by our lab are overlayed in red. The black data points represent previous work by Cantoni et al. [70].

with air this causes a drop in film quality. Because of this, NdBCO shows to be a promising material for devices that need to cycle several times as well as for experiments that require exposure (i.e. low vacuum).

From our experiments we found that our oxygen flow rates were dramatically reduced by almost 90% of that of our standard YBCO growths aswell as EuBCO and GdBCO. As shown by 4.3 inital growth parameters were based on known growth models. However, the oxygen partial pressure was gradually decreased until superconducting films were observed in electrical transport characterization measurements. LAO was chosen for the standard substrate and optimal growth conditions for YBCO were set for a starting point for the deposition runs. As expected, the first run produced an insulating film. As the oxygen flow rate was gradually cut back the films began to superconduct and transition widths got narrower. The final growth parameters were 30 mTorr as a base grow pressure with an argon to oxygen mix ration of 20:1. Substrate temperatures ranged anywhere from

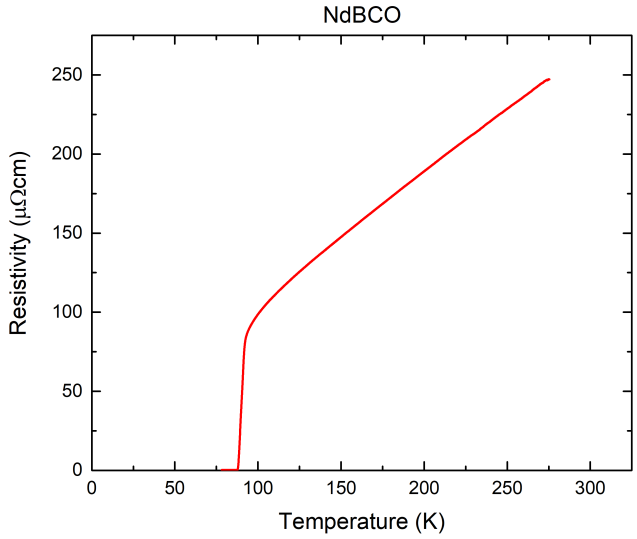

Figure 4.4: Transport data showing a measure of our NdBCO film grown at low oxygen partial pressures. Residual resistivity was extrapolated to 28.2 $\mu\Omega$cm

730 °C to 960 °C with an optimal value of 950 °C being used. In previous studies it was shown that during anneal, a low temperature heat treatment in oxygen increased critical temperature however for our case we quenched the films after growth in high pressure oxygen.

Shown in figure 4.4 is the result of progressions of oxygen reduction in the overall gas mixture during deposition. At high oxygen contents of around 50% oxygen to argon we show films that do not superconduct. As oxygen is finally decreased to about 5% we see metallic behavior in the transport data as well as a sharp transition to superconducting state of the film. This served as the base film model. To investigate effects of substrate choice the chamber was then loaded with 4 new substrates aswell as LAO and ran an identical run as mentioned above. The choice of substrates were as follows; STO, LSAT, NGO, and LAO. NGO peaked our interest because of the shared element neodymium within the substrate and the film. The hope was that with excess elemental neodymium the phase stability line would be shifted and the film would prove more table with respect to wide fluctuations in

oxygen pressures during growth.

The first preliminary run yielded results that did not produce any viable films aside from that grown on LAO. On two samples, NGO and STO it was found that no thin film deposition occurred. This was thought to be due to the substrate temperature being too hot. Because of this it was decided to separately run the different substrates to optimize the growth conditions based on substrate material. The first substrate that had viable thin film deposition was LSAT. It was found that an increase in heater temperature yielded films that were almost as good as those of which we had for our control sample on LAO substrates. With a thermal expansion coefficient of $10 * 10^{-6}T^{-1}$ LSAT was expected to require lower substrate temperatures than that of LAO. However, we found this to be the opposite in terms of data. As substrate temperatures decreased for LSAT we saw a dramatic drop in critical temperature. This led to a hypothesis that NdBCO a lattice mismatch had less of an impact on film quality at higher temperatures when compared to the effect of the substrate material itself. With STO being less effected by substrate temperature and more so by growth pressures. However, by adjusting the growth pressures to try to obtain viable films we began to fall out of the targeted thermal phase stability line. The same was true for the NGO films. Further studies and growth techniques are planned for these two substrates and film combinations. High quality NdBCO thin films on these two particular substrates proved to me the most elusive of all thin film deposition attempts.

We were able to achieve NdBCO film qualities on LSAT that showed transport data equaling and in some cases improving upon the existing NdBCO films on LAO that were used for standard growths for optimising growth conditions. The films deposited on LSAT substrates showed lower residual resistivity as well as showed a lower room temperature resistivity. However, for further transport measurements as grown films on LAO were used. This was done so as to have a standard metric with which to compare with when investigating other cuprates that were grown.

4.3 EuBCO Growth and Characterization

$EuBa_2Cu_3O_{7-\delta}$ (EuBCO) is yet another cuprate studied for growth characteristics as well as film quality in the lanthanide series of interchangeable rare-earth oxides. With an ionic radius of 1.07 (Å) europium is on the larger side of lanthanides studied for rare earth cuprates. Because of this the expectation is to see elevated critical temperatures as well as slightly slower growth rates. Previous studies on EuBCO reveal critical temperatures of around 90 K[80]. Shown in 4.7 is a graph representing europium being on the larger end of ionic radius when compared to most rare earth lanthanides that have been studied for superconducting cuprate thin films. Note the rather small ionic radius of holmium.

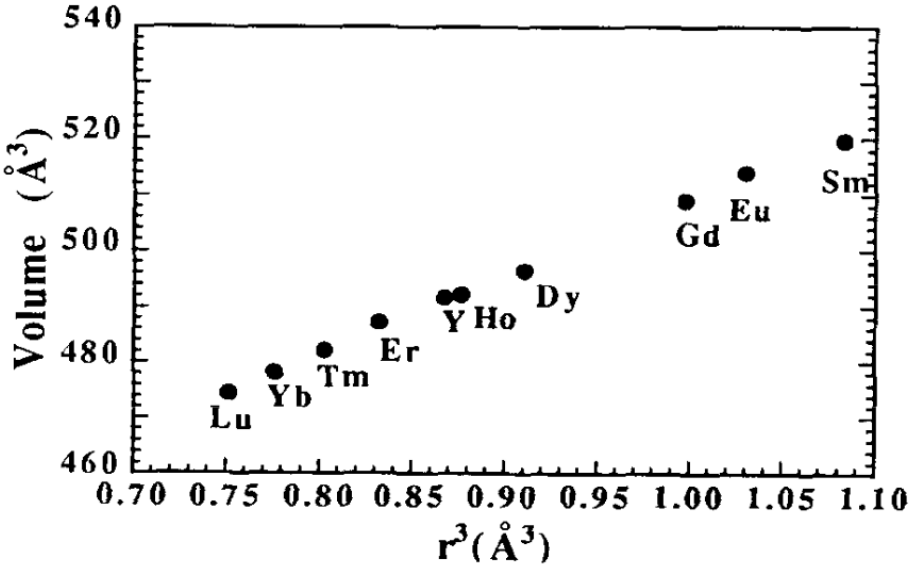

Figure 4.5: A data set showing ionic radius with respect to overall unit cell volume of each cuprate with and substitution of each different lanthanide. Note depicted on this chart is yttrium. Whose ionic radius falls next to holmium. Adapted from [81].

For growth, the chamber was fitted with an invair heater plate with off axis 2 inch sputter guns, both RF and DC. For this growth run we choose to run the DC deposition gun. The target chosen was manufactured by Toshima Manufacturing Ltd. The XRD analysis data confirmed the presence of pure single phase EuBCO. The initial growth conditions were

set at optimal deposition conditions for YBCO as per our previous cuprate growth runs. The first films grown at 800°C with an applied power of 55W to our sputter gun yielded an insulating film. We then began slowly increasing the partial pressure of oxygen to determine if oxygen doping was the cause of bad quality film depositions. When our sputtering gas mixture was almost completely saturated with oxygen we decided to employ our oxygen ion beam. The most successful run of EuBCO deposition came when we pretreated the chamber with oxygen plasma. With no heater or sample installed we pumped down the chamber and started our 5cm Veeco hollow-cathode ion source. With the shutters left up on the sputter guns we ran the hollow cathode oxygen ion source for 35 minutes at a base pressure of $2.5\text{x}10^{-4}$ Torr and an oxygen flow rate of 10 sccm into the body of the gun. The excitation gas (in this case argon) was introduced through the cathode at a rate of 3 sccm. After the initial 35 minutes the gun was switched off and allowed to cool before the sample and heater were loaded into the chamber for growth. After our first depositon run following the oxygen ion pretreatment our initial surface resistance measurements showed we had a viable film. Upon further measurement via 4 point method we found we had a film that had a critical temperature of around 95 K. This is the highest recorded temperature reported to date for EuBCO thin films.

When comparing to bulk YBCO with a critical temperature of around 92K it is clear that EuBCO has an advantage over standard YBCO. As mentioned in previous sections, an enhancement in critical temperature usually is attributed to grain boundaries developed during growth which serve as pinning centers for flux vortices. These flux vortices usually depress critical temperatures in thin film and in bulk. To investigate this further we characterized the same EuBCO thin film in our SEM/EDS system.

For verification of film stoicheometry a point scan was done aswell as line and area scans of the film during SEM imaging. The point scans via EDS showed us the stoichometry suggests these were indeed grains of a cuprate material. In previous studies we showed that in standard YBCO growth, copper-oxide grains begin to form on films. This is usually

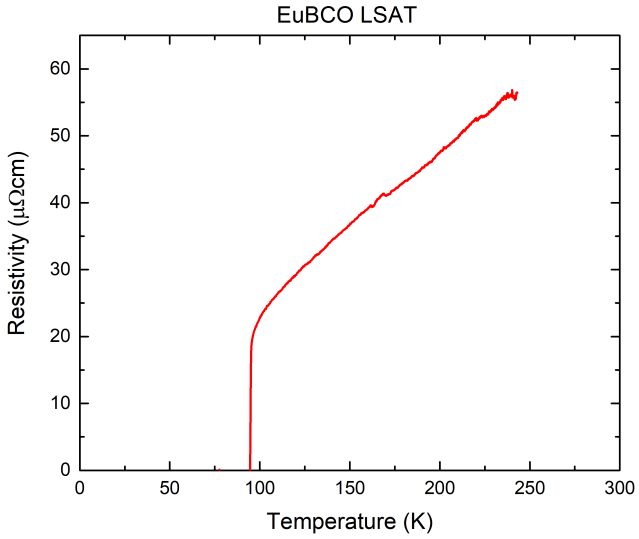

Figure 4.6: Transport data showing the highest critical temperature ever reported for thin film cuprate growth. Resistivity at 250 K is 58$\mu\Omega$cm with a residual resistivity of 3.27 $\mu\Omega$cm. Critical temperature values are within 95 K range.

attributed to high power used on the sputter target or very low low deposition pressures. To determine orientation of the grains as well as composition the Electron Backscattered Diffraction (EBSD detector was used. A large grain around 1 micron was chosen and analyzed with our EBSD detector. We were expecting to find that these large grains were a-axis oriented single crystals which is typical with YBCO films. However, upon analysis we showed that these are in fact c-axis oriented grains of EuBCO. Further studies are expected to determine why a-axis grain formation is not favored as in YBCO growth studies. To determine stoicheometry of the overall film, the area scan was used for EDS and an energy spectrum was obtained. Shown in 4.1 we can see that based on elemental analysis by weight, barium and europium are in good agreement with the optimal ratio of the two in a stable orthorhombic cuprate lattice. The film however seems to be copper rich based on the data at first glance. Given our film was deposited on LSAT for our choosen substrate it is important to note that some of the substrate is factored into the EDS analysis. One reasoning behind the very high copper content shown in the data could be from overalpping

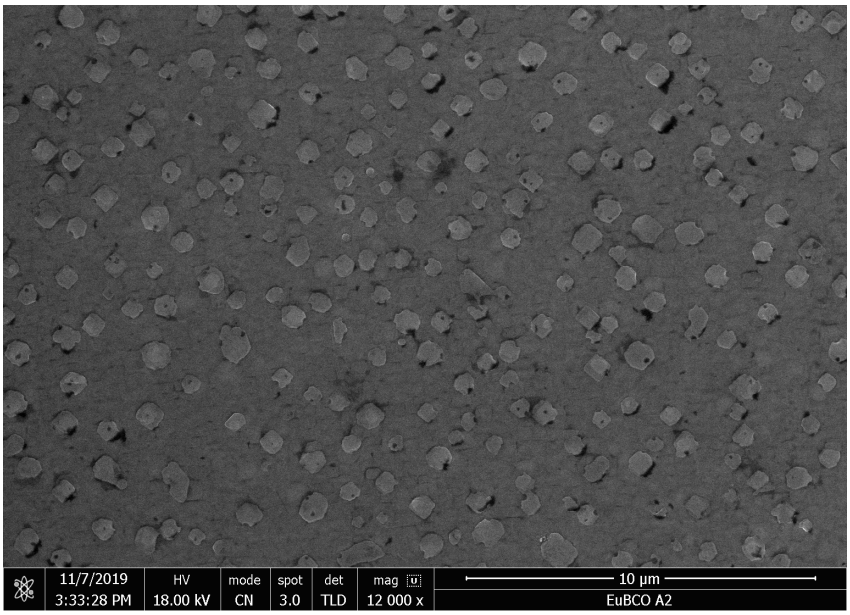

Figure 4.7: SEM imaging of EuBCO surface morphology. As expected, large grains 1 micron wide have developed on the surface. When analyzed by point mode EDS the grains were verified to be epitaxial EuBCO. These large grains are thought to facilitate in the rise of critical temperature that we found during our transport measurements.

2nd order β ionization energies of some of the elements in the substrate with the 1st order α ionization energies of the copper in the film.

Element	Weight %	Weight% Sigma
C	4.01	.064
O	18.26	0.56
Al	4.62	0.19
Cu	14.06	0.58
Sr	18.09	0.73
Ba	7.02	0.54
La	13.55	0.60
Eu	2.55	0.48
Ta	17.86	0.77

Table 4.1: A representation of the overall weights of each element that make up the EuBCO thin film. Important to note are the elements that show up in the energy spectrum related to the substrate LSAT used for this deposition run.

Upon further analysis of each film grown on different subtrates, it was found that

above all other ReBCO thin fimls grown by our group, EuBCO seemed the most sensitive to substrate choice. We were able to successfully grow on NGO, STO, LAO, and LSAT with all of our ReBCO depositon runs. However, despite operating over a wide temperature range and wide oxygen partial pressure we were still unable to successfully deposit EuBCO onto our STO substrates. Contradictory to this finding, some of our best films were produced on LSAT which as mentioned previously is a mixture of both LAO and STO. Further studies as to why this is the case may explain EuBCOs high critical temperature nature when compared to other ReBCO's.

Chapter 5

Superconducting Via and Multilayer Device Design

5.1 Introduction and Motivation

Perhaps the best know superconducting device is a Superconducting Quantum Interference Device (SQUID). This device is analogous to the transistor in semiconducting electronics. The basic building blocks of this device consists of two Josephson junctions connected in parallel forming a loop. When the critical current of the superconducting material is reached, the voltage within the loop starts to flow and begins to oscillate. Because there is a developed voltage a magnetic flux begins to form within the loop. Since there is an existing flux within the loop, any change in this flux will cause a change in voltage. Because of this effect, SQUIDs can be used as very sensitive magnetometers. As stated before, this device can also function to mimic the output of transistor operations. However in this instance, the "gate voltage" on the transistor would be the magnetic flux of the loop. By inducing a magnetic field onto the SQUID loop one could essentially change the voltage to an on-off like state. This inductance coil would be placed directly over the SQUID and can either manipulate the flux of the loop or focus incoming flux to increase sensitivity. In order to successfully couple the inductance coil to the SQUID both the layers

as well as the via connecting the SQUID and the coil need to exhibit superconductivity. Standard vias grown to connect the layers between the insulating barrier would grow with c-axis orientation causing a breakdown in superconductivity. The current multilayer SQUID design is as follows.

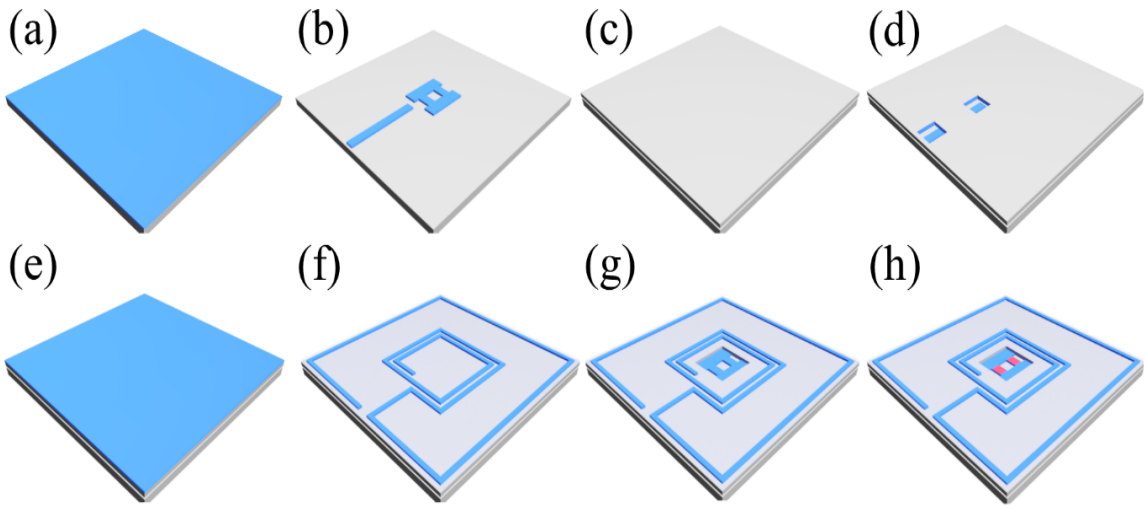

Figure 5.1: A representation of the multilayer SQUID/Flux loop approach. (a) A YBCO deposition onto CeO buffered Al2O3. (b) The SQUID loop pattern is milled. (c) The CeO insulating layer is deposited. (d) A via opening is milled to allow for YBCO a-b plane growth. (e) YBCO flux-loop layer is grown. (f) The flux-loop pattern is milled. (g) A window is milled to allow for beam access to the SQUID. (h) The junction is written with a Helium ion beam.

To circumvent this problem a conductive film of YBCO would be grown on a suitable substrate such as vicinal (STO) discussed the previous section. On the top layer of YBCO a second layer of STO would be grown to serve as the insulating layer. This layer would then be patterned so as to expose half of the surface and etched down to the first layer of detwinned YBCO. To etch to the first layer the sample would be ion milled at an angle in order to achieve a ramp style edge to the STO. This is done so as to prevent a "step-edge" junction from forming during processing. By growing on the STO-YBCO ramp,

the smooth edge transition allows for a consistent film that grows across the preferred a-b lattice plane. Once the second layer of YBCO is grown the two layers will be connected by a superconducting via of the a-b lattice orientation. The inductance coil and the squid could then be patterned. Further studies will be held to find a more suitable substrate/insulating layer with a low dielectric constant such as NGO and LSAT. As stated in the previous section, using a detwinned film with a known crystal orientation would allow us to better tune the characteristics of our device. With a usual flux noise of 10 this value could be decreased with a monocrystalline film. With a decreased flux noise this would allow us to decrease the size of the flux lock loop allowing us to increase our spatial resolution.

5.2 Multilayer Superconducting Via Fabrication

In order to form a superconducting via that would facilitate superconducting transport epitaxial growth in the c-axis direction must be acheived. However, given the properties of "through-vias" the transport would occur in the c-axis direction due to the nature of the growth medium. In this case, the starting substrate is YBCO oriented in the (100) direction. We first elongate the via in order to allow a-b plane growth. To do this, preliminary runs were made using a stacked sample of Sapphire-YBCO-CeO (500nm x 35nm x 20nm thickness respectively). The samples were coated with photo-resist and patterened so as to expose half of the sample and then developed. The samples were then loaded into an argon ion mill and milled for 300 seconds to expose the YBCO ground layer that was capped by the CeO. Special care was taken to stop milling precisely when the YBCO was exposed so as not to degrade the ground layer. Transport measurements were taken of samples before and after milling to ensure the films were not damaged. Each successive sample run in the ion mill was followed by another run with a new sample but with slowly varying angle of incidence with respect to the incoming argon milling beam. This was to determine optimal angle values for epitaxial ramp via formation. Once the samples were milled they were removed from the argon ion mill and all photoresist was removed.

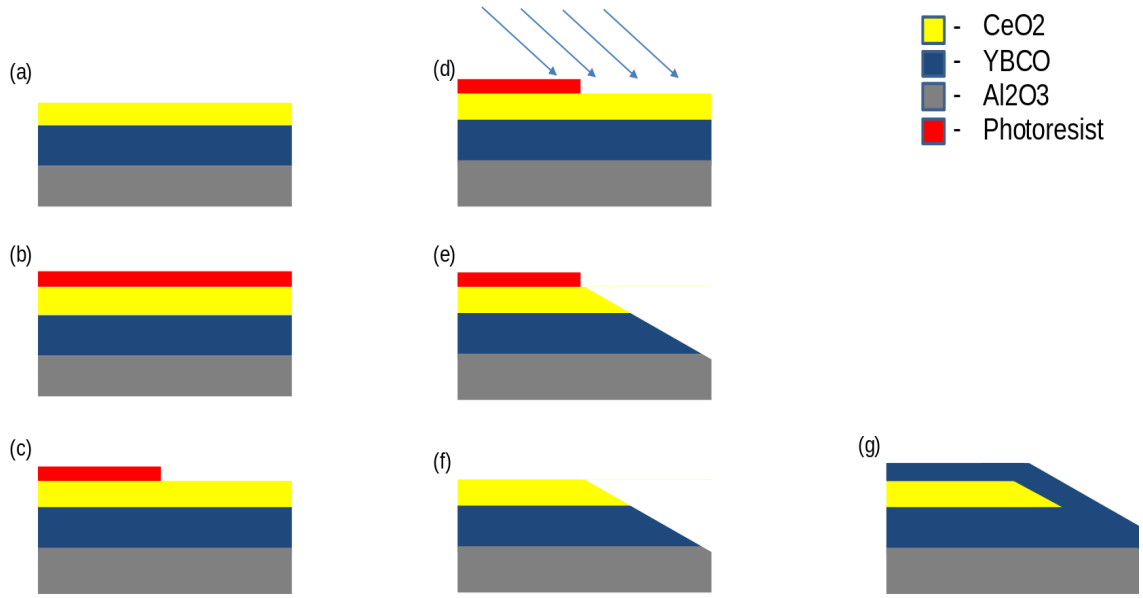

Figure 5.2: A representation of the superconducting via ramp fabrication process.. (a) A YBCO deposition onto CeO buffered Al2O3. (b) Photoresist is spun onto the sample. (c) The resist is patterend to expose the CeO and YBCO. (d) An argon ion beam is introduced to mill into the substrate forming a ramp of CeO and YBCO. (e) The exposed ramp stack down to the substrate (f) The photoresist is removed from the sample exposing the CeO insulating layer. (g) A layer of YBCO is deposited onto the ramp, connecting the bottom layer as well as the top plane above the CeO.

The deposition of the top layer of YBCO had several factors that needed to be taken into consideration when depositing. To achieve growth temperatures it was shown that each thermal cycle drastically effected the transport properties of the ground plane YBCO. This is due to the migration and diffusion of constituents of the substrate into the YBCO as previously mentioned. A new obstacle to overcome was the out-gassing of oxygen from the ground plane YBCO. Because the YBCO is capped with an insulating cerium oxide layer, annealing in high pressure oxygen at high temperatures has little to no effect on the ground plane. Several groups have tried different techniques such as forming "oxygenation vias" through the multilayer stack[82, 83, 84]. This, in theory allows for slow oxygen diffusion throughout the stack during oxygen annealing. While this may have worked well for other groups, it was found that a major contributing factor to the degradation of

the ground layer was most easily circumvented by severely limiting the time the samples were held at growth temperatures that allowed for diffusion and outgassing to occur. Rather than anneal in high pressure oxygen, an oxygen ion beam was switched on briefly before deposition of the top YBCO layer and ramp via. It was shown that transport properties favored a short oxygen ion exposure just prior to deposition compared to those that were not exposed. Once the samples were grown they were allowed to rapidly cool in high pressure oxygen until the reached room temperature and were removed for transport measurements.

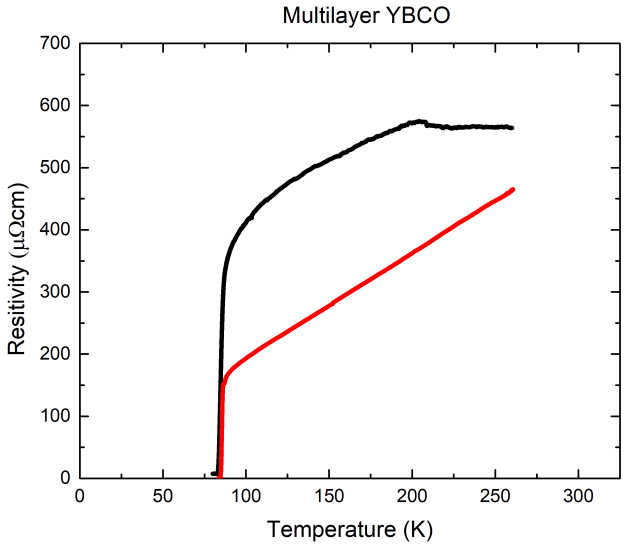

Figure 5.3: Transport data showing a measure of the ground plane YBCO layer shown in red. The film was processed as mentioned and a top YBCO layer connecting through to the ground plane was deposited. The black data represents the top YBCO measured across the ramp.

5.3 Transport Properties and Discussion

To have a standard to base transport measurements off of, the first sample measured was measured through the ground plane to ensure a viable starting point. To do this, contact points were opened up through the cerium oxide capping layer by taking a

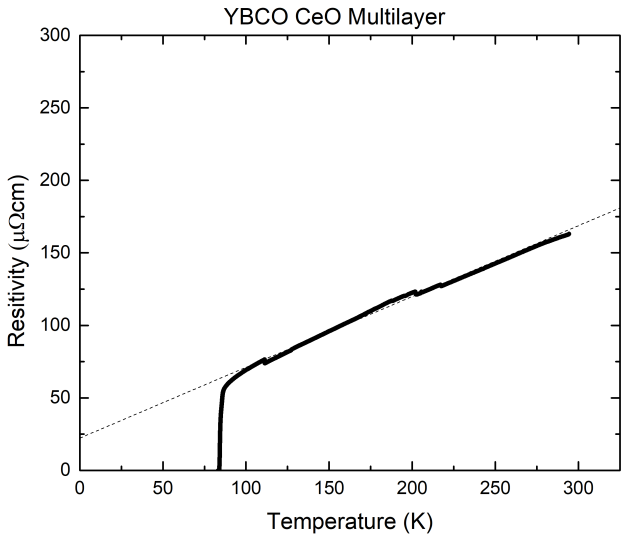

Figure 5.4: Transport data showing a measurement of the top deposited YBCO film. This is to show the film properties of an uninterrupted film across it's base. This film was grown on the cerium oxide capping layer with no ramp milled into the cerium oxide down to the ground plane.

diamond scribe and scratching through the surface. This method was preferred over using the ion mill to reach the ground plane for fear of the ion beam degrading the film and giving inaccurate data sets. The first measurement showed a YBCO thin film of typically quality available commercially. With a resistivity of around 300 $\mu\Omega$cm at room temperature and a residual resistivity value of around 10 $\mu\Omega$cm. For a direct comparison a side by side growth and measurement was made of our thin film deposition properties as well as commercially bought thin films. It was seen that our films not only showed lower residual resistivity but also a lower starting resistivity. This film however was grown on LAO. The next step of the process was to grow directly on the capping layer of cerium oxide. To simulate the effects on the ground plane due to the thermal cycling of growing procedures, the ground plane was measured again after it was brought up to 800 °C and held for the time required for a full deposition run (1 hour). Transport data was taken of this sample and shows a large degradation of film quality when considering electrical transport. This is again, attributed

to lack of oxygen reaching the plane due to the cerium oxide layer during quench annealing in high pressure oxygen. Also, because of the high diffusion rate within the crystal interface at elevated temperatures unwanted compounds form at the substrate/film interface as well as the film/capping layer interface. These factors clearly show that minimal process time and lower temperatures are the most important factors when considering keeping the ground plane YBCO thin film intact. With com partitive electrical transport data taken of the ground plane the as grown YBCO film on the capping layer was then measured for film quality. While keeping pressures relatively high and growth temperatures around 700°C we were able deposit a fairly high quality film of YBCO onto the cerium oxide capping layer. This film was in good agreement with our previous depositions for our standard test samples. Once we established film quality both on the ground plane as well as on top of the cerium oxide capping layer we began trying to grow on the ramp etched samples.

Preliminary results of varying angle of incidents with respect to the incoming ion beam showed us that there is a narrow range in which a top layer of superconducting YBCO is viable. Too steep of an angle and there is a risk that the film will not be continuous and form a barrier. It was found that a range of 15-5° off plane with the film is the optimal milling angle. Our sample milled at 10° showed the most promising results. To measure, we placed the current leads on different levels of the chip. The negative lead was placed on the half of the chip that was stacked YBCO/CeO/YBCO while the positive lead was place on the lower YBCO/YBCO level. This allowed us to investigate transport properties down the ramp to look for signs of any degradation of the film. The residual resistivity was extrapolated to be around 25$\mu\Omega$cm. It is interesting to note that our starting resistivities were much lower than our standard films grown at this thickness. A major contributing factor to this may be in the was the top film develops on the cerium oxide capping layer. When the multilayer stack is brought up to temperature and YBCO is deposited, there is a chance that pin holes can form in the cerium oxide. If this were the case that would mean the thickness of the film would look to through our transport measurements to be twice as thick seeing as the ground plane and top layer would act as one film.

$$\begin{cases} R_s = \frac{\pi R}{ln2} \end{cases} \tag{5.1}$$

In looking at equation 5.1 one can see that the sheet resistance R_s takes into account the resistance of the material multiplied by the Van der Pauw constant. If we have the known sheet resistance from the 4 point measurement and we know the thickness we can calculate resistivity. Show in equation 5.2, the dimensions of the film are used to calculate the resistivity based on the measured values of sheet resistance.

$$\begin{cases} \rho = \frac{l}{A} R \end{cases} \tag{5.2}$$

Where as l is the cross-sectional area of the film we see that the increase in thickness should not give a drop in starting resistance. Therefore we have reason to suspect the ramp has some unexpected result in the effect on electrical transport through the film. Upon further analysis, the sample was characterized via profilometer and SEM. Given the shallow angle of the ramp and the over all surface roughness of the top layer of YBCO, we were unable to get good enough resolution on the profilometer to characterize any ramp feature. SEM results provided us with a detailed structure right at the ramp edge. 5.5 shows a clear indication that the portion of YBCO film that is deposited on the cerium oxide capping layer is drastically different than that of which was deposited on the ground plane YBCO layer. This perhaps could be from the different seed growth during initial deposition. While the cerium oxide requires a 45° off set of the YBCO lattice for growth, the YBCO starting layer allows for direct YBCO lattice matching during deposition. One way to circumvent this would be to have the cerium oxide oriented 45° off the parallel from the edge of the chip during fabrication. This would ensure that our to YBCO layer would have and aligned substrate lattice to deposit on. Not only would this have a positive impact on film quality, it may also allow for better electrical transport properties across the ramp.

Based on the results it is shown that superconducting ramp vias are extremely

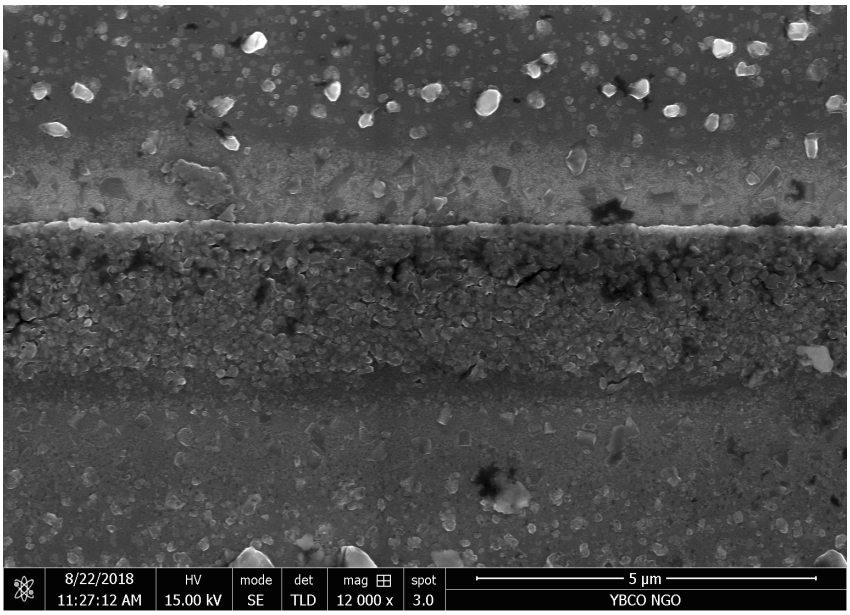

Figure 5.5: SEM top down overview of 10° ramp sample with YBCO deposited. The top portion shows typical YBCO film characteristics of copper-oxide features shown by the high contract spots on the film. The ramp exhibits a sharp boundary line thought to be a-axis oriented film growth. The lower portion grown on the ground plane shows little to no copper-oxide bouldering.

sensitive to ramp angle development. However, more importantly it is shown that keeping the ground plane YBCO layer intact was key in keeping the multilayer stack alive. Based on transport measurements it is shown that there are very different film properties from those which are grown on cerium oxide. Because of this it may be beneficial in future experiments to investigate different insulating layers within the stack such as LAO or STO. Further studies may also be carried out to prove the insulating layer develops no pin hole vias during deposition and processing. With our results seen in 5.4 it is shown that there is an anomaly in the transport data which suggests unwanted contact through the insulating layer from the ground plane to the top YBCO layer may be occurring. Future work is expected for multilayer devices.

Chapter 6

Conclusion

This dissertation describes the results of the ongoing research into high temperature thin film development and device performance. With the recent push in the fields of superconducting quantum electronics as well as quantum information low temperature superconducting electronics have been vetted and are the industries current standards. Because of the large difference in operating temperatures and impedence between conventional silicon electronics and low temperature superconducting circuits it is reasonable to assume a search for more feasible solutions. Because of this, high temperature superconductivity holds yet another promising future. Here presented is a summary of the work into trying to shed light on higher temperature superconducting thin films, novel growth techniques as well as devices. Rare earth superconducting oxides in the form of cuprates have been examined for thin film analysis. Systematic investigations into the outcomes and effects of replacing rare earth elements in the commonly known YBCO crystal structure have been conducted. By replacing the rare earth element yttrium with other novel lanthanides such as holmium and neodymium, different conclusions were drawn than to what is found in most of the available literature on previous studies. It was found that the overall effect of ionic radius within the crystal structure does have an impact on values such as critical currents of junctions as well as film surface stability of exposed samples. It was determined that $HoBa_2Cu_3O_{7-\delta}$ presents a higher critical current density than that of commercially available YBCO films.

Another positive attribute to growing HoBCO is its ability to arrange itself into a near atomically smooth surface for use in crucial devices such as multilayer superconducting quantum interference devices and magnetometers. $NdBa_2Cu_3O_{7-\delta}$ was among the most difficult of all to grow. Owing to the fact that oxygen content of the background gas needed to be an order of magnitude less than that of standard cuprate grows it was found that this particular material responded well to oxygen plasma introduction during the growth process. This hints at a promising nature of deposition for commercial superconducting wires coated with stressed cuprate thin films. Perhaps the most intriguing of all thought my experiments with growing and characterizing rare earth cuprates was that of $EuBa_2Cu_3O_{7-\delta}$. From all respective literature there is no mention of any thin film rare earth cuprate that possessed a critical temperature higher than 92K. Upon growth and characterization of $EuBa_2Cu_3O_{7-\delta}$ it was found to have a critical temperature of 95K. Because of this, it is important to reconsider what was previously thought with respect to ionic radius relating to increases in critical temperatures. Perhaps the most satisfying project involvement was on the oxygen ion beam assisted deposition of rare earth cuprates. Previously unknown in the available literature throughout the past few decades, it is because of this reason unexplored techniques were hypothesized and tested. By applying activated oxygen in situ a decreased surface roughness as well as increased critical temperature was achieved. This previous effect had somewhat of an opposite outcome, when critical temperature increases generally surface roughness also increases. This suggests possible previously unknown phenomena with oxygen plasma during cuprate development and growth which could be applicable in a commercial setting. This also may indicate that there is more at play when considering flux pinning centers and their effect on critical temperature and critical current. This study may give new opportunities to probe the origins of microscopic high temperature superconductivity phenomena and better aid in our understanding of these cuprates as a whole. The other aspect of this project was having hands on knowledge of plasma sources and the ability to operate and modify in real time. By having access and abilities to carry out modifications, experiments were successfully run that were previously hindered by the

current technologies of the day. The outcome of this project shows a potential new avenue in high temperature thin film development as well as superconducting circuit processing. Potentially bringing high temperature cuprates once again to the forefront of research and development.

Bibliography

[1] Maw-Kuen Wu, Jo R Ashburn, ClJ Torng, Ph H Hor, Rl L Meng, Lo Gao, Z Jo Huang, YQ Wang, and aCW Chu. Superconductivity at 93 k in a new mixed-phase y-ba-cu-o compound system at ambient pressure. *Physical review letters*, 58(9):908, 1987.

[2] D Dimos, P Chaudhari, and J Mannhart. Superconducting transport properties of grain boundaries in yba 2 cu 3 o 7 bicrystals. *Physical Review B*, 41(7):4038, 1990.

[3] Alice E White, KT Short, RC Dynes, AFJ Levi, M Anzlowar, KW Baldwin, PA Polakos, TA Fulton, and LN Dunkleberger. Controllable reduction of critical currents in yba2cu3o7- δ films. *Applied physics letters*, 53(11):1010–1012, 1988.

[4] T Scherer, P Marienhoff, R Herwig, M Neuhaus, and W Jutzi. Anisotropy on the a, b-plane of c-axis orientated almost twin-free ybco films on ndgao3. *Physica C: Superconductivity*, 197(1-2):79–83, 1992.

[5] John R Hardy and John W Flocken. Possible origins of high-t c superconductivity. *Physical review letters*, 60(21):2191, 1988.

[6] JP Franck and DD Lawrie. The copper isotope effect in oxygen-deficient yba 2 cu 3 o 7- δ. *Journal of superconductivity*, 8(5):591–594, 1995.

[7] ZG Ivanov, EA Stepantsov, T Claeson, F Wenger, SY Lin, N Khare, and P Chaudhari. Highly anisotropic supercurrent transport in yba 2 cu 3 o 7- δ bicrystal josephson junctions. *Physical Review B*, 57(1):602, 1998.

[8] Hiroshi Akoh, Fujitoshi Shinoki, Masayuki Takahashi, and Susumu Takada. Sns josephson junction consisting of y-ba-cu-o/au/nb thin films. *Japanese journal of applied physics*, 27(4A):L519, 1988.

[9] JM Valles Jr, AE White, KT Short, RC Dynes, JP Garno, AFJ Levi, M Anzlowar, and K Baldwin. Ion-beam-induced metal-insulator transition in y ba 2 cu 3 o 7- δ: A mobility edge. *Physical Review B*, 39(16):11599, 1989.

[10] PK Gallagher. Hm. o'bryan. sa sunshinr. and dw murphy. *Mat. Res. Bull*, 22:995, 1987.

[11] Robert Joseph Cava, B Batlogg, Ch H Chen, EA Rietman, SM Zahurak, and D Werder. Single-phase 60-k bulk superconductor in annealed ba 2 y cu 3 0 7- δ (0.3¡ δ¡ 0.4) with correlated oxygen vacancies in the cu-o chains. *Physical Review B*, 36(10):5719, 1987.

[12] Takanobu Kiss, T Matsushita, and F Irie. Relationship among flux depinning, irreversibility and phase transition in a disordered hts material. *Superconductor Science and Technology*, 12(12):1079, 1999.

[13] Alice E White, KT Short, DC Jacobson, JM Poate, RC Dynes, PM Mankiewich, WJ Skocpol, RE Howard, M Anzlowar, KW Baldwin, et al. Ion-beam-induced destruction of superconducting phase coherence in yba 2 cu 3 o 7- δ. *Physical Review B*, 37(7):3755, 1988.

[14] P Xiong, AV Herzog, and RC Dynes. Superconductivity in ultrathin quench-condensed pb/sb and pb/ge multilayers. *Physical Review B*, 52(5):3795, 1995.

[15] L Merchant, J Ostrick, RP Barber Jr, and Robert C Dynes. Crossover from phase fluctuation to amplitude-dominated superconductivity: A model system. *Physical Review B*, 63(13):134508, 2001.

[16] JM Valles and RC Dynes. Superconductivity and tunneling spectroscopy in granular and homogeneous quench condensed thin films. *MRS Online Proceedings Library Archive*, 195, 1990.

[17] Shane A Cybart, Patricia XT Yen, Ethan Y Cho, Jeong Uk Huh, VN Glyantsev, Christopher S Yung, Brian Moeckly, Jeffrey W Beeman, and Robert C Dynes. Comparison of y–ba–cu–o films irradiated with helium and neon ions for the fabricationof josephson devices. *IEEE Transactions on Applied Superconductivity*, 24(4):1–5, 2014.

[18] DE McCumber. Effect of ac impedance on dc voltage-current characteristics of superconductor weak-link junctions. *Journal of Applied Physics*, 39(7):3113–3118, 1968.

[19] WC Stewart. Current-voltage characteristics of josephson junctions. *Applied Physics Letters*, 12(8):277–280, 1968.

[20] Mohit Randeria, Nandini Trivedi, Adriana Moreo, and Richard T Scalettar. Pairing and spin gap in the normal state of short coherence length superconductors. *Physical review letters*, 69(13):2001, 1992.

[21] G Nieva, E Osquiguil, J Guimpel, M Maenhoudt, B Wuyts, Y Bruynseraede, MB Maple, and Ivan K Schuller. Photoinduced changes in the transport properties of oxygen-deficient yba 2 cu 3 o x. *Physical Review B*, 46(21):14249, 1992.

[22] JQ Zheng, MC Shih, S Williams, SJ Lee, Hiroshi Kajiyama, XK Wang, Z Zhao, K Viani, S Jacobson, Pulak Dutta, et al. Effect of oxygen partial pressure on the in situ growth of y-ba-cu-o thin films on srtio3. *Applied physics letters*, 59(2):231–233, 1991.

[23] Mitsumasa Suzuki, Yogesh Soman, Ed Tarte, Peter Berghuis, and Jan Evetts. Preparation and properties of c-axis-oriented ndba2cu3o7- δ films by dc sputtering. *Physica C: Superconductivity*, 312(3-4):191–196, 1999.

[24] W Jo, LS-J Peng, W Wang, T Ohnishi, AF Marshall, RH Hammond, MR Beasley, and EJ Peterson. Thermodynamic stability and kinetics of y–ba–cu–o film growth at high rates in atomic and molecular oxygen. *Journal of crystal growth*, 225(2-4):183–189, 2001.

[25] N Terada, CH Ahn, D Lew, Y Suzuki, KE Kihlstrom, KB Do, SB Arnason, TH Geballe, RH Hammond, and MR Beasley. Surface study of yba2cu3o7- δ epitaxial films cleaned by an atomic oxygen beam. *Applied physics letters*, 64(19):2581–2583, 1994.

[26] AC Westerheim, LS Yu-Jahnes, and Alfredo C Anderson. Off-axis magnetron sputtering of ybco films: The influence of atomic oxygen. *IEEE Transactions on Magnetics*, 27(2):1001–1005, 1991.

[27] Robert H Hammond, Vladimir Matijasevic, and Rüdiger Bormann. Correlation between in situ growth conditions and thermodynamic stability criteria for y 1 ba 2 cu 3 o y. In *Science and Technology of Thin Film Superconductors 2*, pages 395–401. Springer, 1990.

[28] R Bormann and J Nölting. Stability limits of the perovskite structure in the y-ba-cu-o system. *Applied Physics Letters*, 54(21):2148–2150, 1989.

[29] SR Foltyn, P Tiwari, RC Dye, MQ Le, and XD Wu. Pulsed laser deposition of thick yba2cu3o7- δ films with j c 1 ma/cm2. *Applied physics letters*, 63(13):1848–1850, 1993.

[30] QX Jia, SR Foltyn, PN Arendt, and JF Smith. High-temperature superconducting thick films with enhanced supercurrent carrying capability. *Applied physics letters*, 80(9):1601–1603, 2002.

[31] N Inoue, W Nishikawa, T Yamamoto, and Y Yasuoka. Surface smoothness of ybco thin-films deposited by rf-sputtering. *Vacuum*, 46(12):1381–1384, 1995.

[32] Paola Benzi, Elena Bottizzo, and Nicoletta Rizzi. Oxygen determination from cell dimensions in ybco superconductors. *Journal of Crystal Growth*, 269(2-4):625–629, 2004.

[33] Jinhua Ye and Keikichi Nakamura. Quantitative structure analyses of yba 2 cu 3 o 7- δ thin films: Determination of oxygen content from x-ray-diffraction patterns. *Physical Review B*, 48(10):7554, 1993.

[34] Zhenghe Han, U Helmersson, TI Selinder, and J-E Sundgren. X-ray-diffraction mapping of epitaxial yba 2 cu 3 o 7- x thin films: Determination of in-plane epitaxy and a-, b-, and c-axis lengths in films with varying oxygen deficiency. *Physical Review B*, 47(6):3431, 1993.

[35] Bernd Stritzker, J Schubert, U Poppe, W Zander, U Krüger, A Lubig, and Ch Buchal. Comparison of ybco-films prepared by laser ablation and sputtering. *Journal of the Less Common Metals*, 164:279–291, 1990.

[36] T Scherer, R Herwig, P Marienhoff, M Neuhaus, A Vogt, and W Jutzi. Off-axis sputtered y1ba2cu3o7-δ films on ndgao3. *Cryogenics*, 31(11):975–978, 1991.

[37] Y Vygranenko, K Wang, M Vieira, and A Nathan. Indium oxide thin-film transistor by reactive ion beam assisted deposition. *physica status solidi (a)*, 205(8):1925–1928, 2008.

[38] HJ Shin, YJ Cho, JY Won, HJ Kang, CH Baeg, JW Hong, and MY Wey. Change of preferred orientation in tin thin films grown by ultrahigh vacuum reactive ion beam assisted deposition. *Nuclear Instruments and Methods in Physics Research Section B: Beam Interactions with Materials and Atoms*, 190(1-4):807–812, 2002.

[39] Philip J Martin, H Angus MacLeod, Roger P Netterfield, CG Pacey, and Wayne G Sainty. Ion-beam-assisted deposition of thin films. *Applied Optics*, 22(1):178–184, 1983.

[40] L Dong and DJ Srolovitz. Texture development mechanisms in ion beam assisted deposition. *Journal of applied physics*, 84(9):5261–5269, 1998.

[41] Kenji Gamo, Nobuyuki Takakura, Norihiko Samoto, Ryuichi Shimizu, and Susumu Namba. Ion beam assisted deposition of metal organic films using focused ion beams. *Japanese journal of applied physics*, 23(5A):L293, 1984.

[42] Robert N Varney. Monatomic and diatomic ions in oxygen. *Physical Review A*, 2(2):370, 1970.

[43] M Tachiki and S Takahashi. Strong vortex pinning intrinsic in high-tc oxide superconductors. *Solid state communications*, 70(3):291–295, 1989.

[44] A Walkenhorst, C Tome-Rosa, C Stölzel, G Jakob, M Schmitt, and H Adrian. Anisotropy of the depinning field and the pinning force density of thin epitaxial yba2cu3o7 films. *Physica C: Superconductivity*, 177(1-3):165–170, 1991.

[45] DH Lowndes, DK Christen, CE Klabunde, Zhong Lin Wang, DM Kroeger, JD Budai, Shen Zhu, and DP Norton. Strong, asymmetric flux pinning by miscut-growth-initiated columnar defects in epitaxial yba 2 cu 3 o 7- x films. *Physical review letters*, 74(12):2355, 1995.

[46] S Hontsu, J Ishii, T Kawai, and S Kawai. Lasrgao4 substrate gives oriented crystalline yba2cu3o7- y films. *Applied physics letters*, 59(22):2886–2888, 1991.

[47] Y Suzuki, D Lew, AF Marshall, MR Beasley, and TH Geballe. Anisotropic transport properties of in-plane-aligned a-axis yba 2 cu 3 o 7 films. *Physical Review B*, 48(14):10642, 1993.

[48] Saburo Tanaka and Hideo Itozaki. High-jc superconducting single crystalline hobacuo thin films by sputtering. *Japanese journal of applied physics*, 27(4A):L622, 1988.

[49] CNR Rao, P Ganguly, J Gopalakrishnan, and DD Sarma. Mechanism of high-temperature superconductivity in yba2cu3o7- δ: Crucial role of oxygen. *Materials research bulletin*, 22(8):1159–1163, 1987.

[50] Robert Poole. New superconductors answer some questions. *Science*, 240(4849):146–148, 1988.

[51] Jean-Marie Tarascon, WR McKinnon, LH Greene, GW Hull, Vogel, and EM. Oxygen and rare-earth doping of the 90-k superconducting perovskite yba 2 cu 3 o 7- x. *Physical Review B*, 36(1):226, 1987.

[52] M Sugano, K Osamura, W Prusseit, R Semerad, K Itoh, and T Kiyoshi. Intrinsic strain effect on critical current and its reversibility for ybco coated conductors with different buffer layers. *Superconductor Science and Technology*, 18(3):369, 2005.

[53] Michinaka Sugano, Kouji Shikimachi, Naoki Hirano, and Shigeo Nagaya. The reversible strain effect on critical current over a wide range of temperatures and magnetic fields for ybco coated conductors. *Superconductor Science and Technology*, 23(8):085013, 2010.

[54] HY Zhai and WK Chu. Effect of interfacial strain on critical temperature of yba 2 cu 3 o 7- δ thin films. *Applied Physics Letters*, 76(23):3469–3471, 2000.

[55] J Colino, JL Sacedon, and JL Vicent. Study of the oxygen depletion in the film-substrate interface of superconducting yba2cu3o7- x films. *Applied physics letters*, 59(25):3327–3329, 1991.

[56] DB Fenner, AM Viano, DK Fork, GAN Connell, JB Boyce, FA Ponce, and JC Tramontana. Reactions at the interfaces of thin films of y-ba-cu-and zr-oxides with si substrates. *Journal of applied physics*, 69(4):2176–2182, 1991.

[57] Haibin Su, David O Welch, and Winnie Wong-Ng. Strain effects on point defects and chain-oxygen order-disorder transition in 123 cuprate compounds. *Physical Review B*, 70(5):054517, 2004.

[58] Lisa A Tietz, C Barry Carter, Daniel K Lathrop, Stephen E Russek, Robert A Buhrman, and Joseph R Michael. Crystallography of yba 2 cu 3 o 6+ x thin film-substrate interfaces. *Journal of Materials Research*, 4(5):1072–1081, 1989.

[59] M Guillaume, P Allenspach, J Mesot, B Roessli, U Staub, P Fischer, and A Furrer. A systematic neutron diffraction study of rba 2 cu 3 o 7 (r= yttrium and rare earths) high-t c superconductors. *Zeitschrift für Physik B Condensed Matter*, 90(1):13–17, 1993.

[60] C Andreouli and A Tsetsekou. Synthesis of htsc re (y) ba2cu3ox powders: the role of ionic radius. *Physica C: Superconductivity*, 291(3-4):274–286, 1997.

[61] Shane A Cybart, EY Cho, TJ Wong, Björn H Wehlin, Meng K Ma, Chuong Huynh, and RC Dynes. Nano josephson superconducting tunnel junctions in yba 2 cu 3 o 7–δ directly patterned with a focused helium ion beam. *Nature nanotechnology*, 10(7):598, 2015.

[62] Saburo Tanaka and Hideo Itozaki. Crystallinity and morphology of superconducting thin films prepared by sputtering. *Japanese Journal of Applied Physics*, 28(3A):L441, 1989.

[63] MI Faley, U Poppe, K Urban, DN Paulson, and RL Fagaly. A new generation of the hts multilayer dc-squid magnetometers and gradiometers. In *Journal of Physics: Conference Series*, volume 43, page 1199. IOP Publishing, 2006.

[64] JT Jeng, Herng-Er Horng, and Hong-Chang Yang. High-tc squid magnetometers and gradiometers for nde application. *Physica C: Superconductivity*, 368(1-4):105–108, 2002.

[65] Henry Y Luo, Quentin P Herr, Randall M Burnett, and Donald L Miller. Superconducting memory system with stacked drivers and differential transformers, February 12 2019. US Patent 10,204,677.

[66] Roman Caudillo, Lester Lampert, David J Michalak, Jeanette M Roberts, Ravi Pillarisetty, Hubert C George, Nicole K Thomas, and James S Clarke. Vertical flux bias lines coupled to vertical squid loops in superconducting qubits, February 7 2019. US Patent App. 16/102,780.

[67] K Inoue, N Takeuchi, K Ehara, Y Yamanashi, and N Yoshikawa. Simulation and experimental demonstration of logic circuits using an ultra-low-power adiabatic quantum-flux-parametron. *IEEE Transactions on Applied Superconductivity*, 23(3):1301105–1301105, 2012.

[68] Daimeng Zhang, Melissa Trepanier, Oleg Mukhanov, and Steven M Anlage. Tunable broadband transparency of macroscopic quantum superconducting metamaterials. *Physical Review X*, 5(4):041045, 2015.

[69] M Ciszek, J Olejniczak, E Trojnar, AJ Zaleski, J Klamut, AJM Roovers, and LJM Van de Klundert. Ac losses and critical current density of superconducting gdba2cu3o7- x. *Physica C: Superconductivity*, 152(3):247–250, 1988.

[70] C Cantoni, DP Norton, DM Kroeger, M Paranthaman, DK Christen, D Verebelyi, R Feenstra, DF Lee, ED Specht, V Boffa, et al. Phase stability for the in situ growth of nd 1+ x ba 2- x cu 3 o y films using pulsed-laser deposition. *Applied physics letters*, 74(1):96–98, 1999.

[71] P Yossefov, GE Shter, GM Reisner, A Friedman, Y Yeshurun, and GS Grader. Relationship of solubility parameter (x), powder properties and phase formation in the nd1+ xba2- xcu3o6. 5+ x2+ δ system. *Physica C: Superconductivity*, 275(3-4):299–310, 1997.

[72] In-Seon Kim, Kyu Won Lee, Yong Ki Park, and Jong-Chul Park. Properties of ndba2cu3o7- δ thin film prepared by off-axis rf sputtering. *Applied physics letters*, 68(13):1859–1861, 1996.

[73] M Badaye, Wu Ting, K Fukushima, N Koshizuka, T Morishita, and S Tanaka. Scanning probe microscopy of ndba2cu3o x thin film surfaces. *Applied physics letters*, 67(15):2155–2157, 1995.

[74] M Badaye, JG Wen, K Fukushima, N Koshizuka, T Morishita, T Nishimura, and Y Kido. Superior properties of over thin films. *Superconductor Science and Technology*, 10(11):825, 1997.

[75] H Behner, K Rührnschopf, G Wedler, and W Rauch. Surface reactions and long time stability of ybco thin films. *Physica C: Superconductivity*, 208(3-4):419–424, 1993.

[76] Temel H Büyüklimanli and Joseph H Simmons. Surface degradation of yba 2 cu 3 o 7- δ superconductors on exposure to air and humidity. *Physical Review B*, 44(2):727, 1991.

[77] JG Lin, CY Huang, YY Xue, CW Chu, XW Cao, and JC Ho. Origin of the r-ion effect on t c in r ba 2 cu 3 o 7. *Physical Review B*, 51(18):12900, 1995.

[78] Seung-Hyun Moon and Byungdu Oh. Ndba2cu3o7-δ superconducting thin films made by the pld method. *Physica C: Superconductivity*, 282:677–678, 1997.

[79] Kôki Takita, Hiroyuki Akinaga, Hideo Katoh, Hajime Asano, and Kohzoh Masuda. Hole concentration compensation effect and superconducting properties of nd1+ xba2-xcu3o7-δ. *Japanese journal of applied physics*, 27(1A):L67, 1988.

[80] C Cai, B Holzapfel, J Hänisch, L Fernandez, and L Schultz. High critical current density and its field dependence in mixed rare earth (nd, eu, gd) ba 2 cu 3 o 7- δ thin films. *Applied physics letters*, 84(3):377–379, 2004.

[81] A Salinas-Sanchez, JL Garcia-Munoz, J Rodriguez-Carvajal, R Saez-Puche, and JL Martinez. Structural characterization of r2bacuo5 (r= y, lu, yb, tm, er, ho, dy, gd, eu and sm) oxides by x-ray and neutron diffraction. *Journal of Solid State Chemistry*, 100(2):201–211, 1992.

[82] G Ockenfuβ, R Wördenweber, TA Scherer, R Unger, and W Jutzi. In-situ low pressure oxygen annealing of yba2cu3o7- δ single-and multilayer systems. *Physica C: Superconductivity*, 243(1-2):24–28, 1995.

[83] BR David, D Grundler, R Eckart, K Fanghanel, JP Krumme, V Doormann, and O Dossel. A multi-layer process for the fabrication of htsc flux transformers and squids. *Superconductor Science and Technology*, 7(5):287, 1994.

[84] Masahiro Horibe, Hironori Wakana, Yoshihiro Ishimaru, Seiji Adachi, Yoshinobu Tarutani, and Kiichi Tanabe. Optimization of fabrication conditions for multilayer structures with la-doped ybco groundplane. *IEEE transactions on applied superconductivity*, 13(2):787–790, 2003.

[85] J Button-Shafer, RL Lichti, and WH Potter. High proton polarization achieved with a (yb, y)(c 2 h 5 s o 4) 3· 9 h 2 o spin refrigerator in a nonuniform magnetic field. *Physical Review Letters*, 39(11):677, 1977.

[86] K Char, MS Colclough, SM Garrison, Nathan Newman, and G Zaharchuk. Bi-epitaxial grain boundary junctions in yba2cu3o7. *Applied physics letters*, 59(6):733–735, 1991.

[87] Yuriy Divin and Ulrich Poppe. Towards "ideal" high-tc josephson junction:[100]-tilt yba2cu3o7-x bicrystal boundary. *Physics Procedia*, 36:42–47, 2012.

[88] Akira Fujimaki, Kouichi Kawai, Noriyoshi Hayashi, Masahiro Horibe, Michitaka Maruyama, and Hisao Hayakawa. Preparation of ramp-edge josephson junctions with natural barriers. *IEEE transactions on applied superconductivity*, 9(2):3436–3439, 1999.

[89] Brian David Josephson. Possible new effects in superconductive tunnelling. *Physics letters*, 1(7):251–253, 1962.

[90] Dieter Koelle, R Kleiner, F Ludwig, E Dantsker, and John Clarke. High-transition-temperature superconducting quantum interference devices. *Reviews of Modern Physics*, 71(3):631, 1999.

[91] CP Foley, EE Mitchell, SKH Lam, B Sankrithyan, YM Wilson, DL Tilbrook, and SJ Morris. Fabrication and characterisation of ybco single grain boundary step edge junctions. *IEEE transactions on applied superconductivity*, 9(2):4281–4284, 1999.

[92] BH Moeckly and K Char. Properties of interface-engineered high t c josephson junctions. *Applied physics letters*, 71(17):2526–2528, 1997.

[93] J Hollkott, S Hu, C Becker, J Auge, B Spangenberg, and H Kurz. Combined method of electron-beam lithography and ion implantation techniques for the fabrication of high-temperature superconductor josephson junctions. *Journal of Vacuum Science & Technology B: Microelectronics and Nanometer Structures Processing, Measurement, and Phenomena*, 14(6):4100–4104, 1996.

[94] D-J Kang, NH Peng, R Webb, C Jeynes, G Burnell, JH Yun, SH Moon, B Oh, EJ Tarte, DF Moore, et al. Irradiation damage technology for manufacturable josephson junctions. *Nuclear Instruments and Methods in Physics Research Section B: Beam Interactions with Materials and Atoms*, 188(1-4):183–188, 2002.

[95] Shane A Cybart, Ke Chen, and RC Dynes. Planar yba/sub 2/cu/sub 3/o/sub 7-/spl delta//ion damage josephson junctions and arrays. *IEEE transactions on applied superconductivity*, 15(2):241–244, 2005.

[96] Shane A Cybart, Peter Roediger, Ke Chen, JM Parker, Ethan Y Cho, Travis J Wong, and Robert C Dynes. Temporal stability of y–ba–cu–o nano josephson junctions from ion irradiation. *IEEE Transactions on Applied Superconductivity*, 23(3):1100103–1100103, 2012.

[97] S Tanaka, T Nakamura, M Iiyama, N Yoshida, S Takano, F Shoji, and K Oura. Low-energy ion scattering spectroscopy observations of c-axis-oriented yba2cu3o7- x thin films: Effects of in-vacuum annealing. *Applied physics letters*, 59(27):3637–3639, 1991.

[98] Ke Chen, Shane A Cybart, and RC Dynes. Study of closely spaced yba/sub 2/cu/sub 3/o/sub 7-/spl delta//josephson junction pairs. *IEEE Transactions on applied superconductivity*, 15(2):149–152, 2005.

[99] J Doherty, B Ward, and E Kellogg. Focused ion beams in microelectronic fabrication. *IEEE transactions on components, hybrids, and manufacturing technology*, 6(3):329–333, 1983.

[100] RL Seliger, RL Kubena, RD Olney, JW Ward, and V Wang. High-resolution, ion-beam processes for microstructure fabrication. *Journal of Vacuum Science and Technology*, 16(6):1610–1612, 1979.

[101] Chiu-Hsien Wu, Yu-Te Chou, Wei-Cheng Kuo, Jau-Han Chen, Li-Min Wang, Ji-Cheng Chen, Kuen-Lin Chen, Un-Cheong Sou, Hong-Chang Yang, and Jen-Tzong Jeng. Fabrication and characterization of high-tc yba2cu3o7- x nanosquids made by focused ion beam milling. *Nanotechnology*, 19(31):315304, 2008.

[102] FHM Rahman, Shawn McVey, Louis Farkas, John A Notte, Shida Tan, and Richard H Livengood. The prospects of a subnanometer focused neon ion beam. *Scanning*, 34(2):129–134, 2012.

[103] BW Ward, John A Notte, and NP Economou. Helium ion microscope: A new tool for nanoscale microscopy and metrology. *Journal of Vacuum Science & Technology B: Microelectronics and Nanometer Structures Processing, Measurement, and Phenomena*, 24(6):2871–2874, 2006.

[104] Katsuhiro Suma, Takahiro Tsuruda, Hideto Hidaka, Takahisa Eimori, Toshiyuki Oashi, Yasuo Yamaguchi, Toshiaki Iwamatsu, Masakazu Hirose, Fukashi Morishita, Kazutami Arimoto, et al. An soi-dram with wide operating voltage range by cmos/simox technology. *IEEE Journal of Solid-State Circuits*, 29(11):1323–1329, 1994.

[105] Y Soutome, R Hanson, T Fukazama, K Saitoh, A Tsukamoto, Y Tarutani, and K Takagi. Investigation of ramp-type josephson junctions with surface-modified barriers. *IEEE transactions on applied superconductivity*, 11(1):163–166, 2001.

[106] QD Jiang and J Zegenhagen. Srtio3 (001) surfaces and growth of ultra-thin gdba2cu3o7- x films studied by leed/aes and uhv-stm. *Surface science*, 338(1-3):L882–L888, 1995.

[107] DH Tran, WBK Putri, CH Wie, B Kang, NH Lee, WN Kang, JY Lee, and WK Seong. Enhanced critical current density in gdba2cu3o7- δ thin films with substrate surface decoration using gd2o3 nanoparticles. *Thin Solid Films*, 526:241–245, 2012.

[108] K Miyachi, K Sudoh, Y Ichino, Y Yoshida, and Y Takai. The effect of the substitution of gd for ba site on gd1+ xba2- xcu3o6+ δ thin films. *Physica C: Superconductivity*, 392:1261–1264, 2003.

[109] SH Song, KP Ko, RK Ko, KJ Song, SH Moon, and SI Yoo. High-jc gdba2cu3o7 thin films on srtio3 substrates by pulsed laser deposition. *Physica C: Superconductivity and its applications*, 463:497–500, 2007.

[110] XW Cao, J Fang, ZH Wang, XJ Xu, RL Wang, and HC Li. Two-dimensional properties of gdba 2 cu 3 o 7- δ epitaxial thin films. *Physical Review B*, 56(13):8341, 1997.

[111] Michael Rudolf Koblischka, AJJ Van Dalen, T Higuchi, SI Yoo, and Masato Murakami. Analysis of pinning in ndba 2 cu 3 o 7- δ superconductors. *Physical Review B*, 58(5):2863, 1998.

[112] H Wu, MJ Kramer, KW Dennis, and RW McCallum. Effect of oxygen partial pressure on the lower solubility limit of nd1+ xba2- xcu3o7. *Physica C: Superconductivity*, 290(3-4):252–264, 1997.